Magnetic, transport, and optical properties of monolayer copper oxides

M. A. Kastner and R. J. Birgeneau

Department of Physics and Center for Materials Science and Engineering, Massachusetts Institute of Technology, Cambridge, Massachusetts 02139

G. Shirane

Brookhaven National Laboratory, Upton, New York 11973

Y. Endoh

Department of Physics, Tohoku University, Aramaki Aoba, Aoba-ku, Sendai 980, Japan

The authors review the results of a wide variety of experiments on materials such as La_2CuO_4 and Nd_2CuO_4 that contain weakly coupled CuO_2 layers. These materials are antiferromagnetic insulators with very large Heisenberg exchange energies, which become high-temperature superconductors when charge carriers are added to the CuO_2 layers. The growth of large single crystals has made it possible to carry out neutron scattering, as well as anisotropic optical, transport, and magnetization measurements. The properties of the undoped CuO_2 layer are reviewed, and the evolution of magnetic, optical, and transport properties with the addition of charge carriers is discussed. The emphasis is on the pure and lightly doped materials, although the magnetism in the superconductors is discussed. [S0034-6861(98)00403-6]

CONTENTS

I. INTRODUCTION

For decades it has been known that the transition-metal oxides display a wide variety of exotic behaviors. There are compounds that undergo insulator-to-metal transitions as a function of pressure or temperature; others that transform from antiferromagnetic insulators to ferromagnetic metals as a function of doping; and many that exhibit structural phase transitions. Whereas there has been much success in developing a theory of the structural phase transitions, the insulator-to-metal transition and the concomitant evolution of the magnetism remains one of the great unsolved problems in condensed-matter physics. The latter problem is extremely difficult because the insulating state in these materials results from the highly correlated motion of the electrons in the d orbitals of the transition elements. The discovery by Bednorz and Müller of high-temperature superconductivity in the layered copper oxides (Bednorz and Müller, 1986) reinvigorated the search for an understanding of the insulator-to-metal transition because it is widely believed that the same correlations that lead to the insulating state, for which the charge-carrier density is small, also lead to superconductivity when the carrier density is sufficiently large.

The approach we have taken since the discovery of high-T_c superconductivity is to study the evolution of the transport and magnetic properties as a function of carrier density beginning with the antiferromagnetic insulator and working our way into the superconducting phase. Some in the superconductivity community argue that the mechanism of the new superconductivity can be identified most readily by studying the materials either with the highest critical temperatures (T_c) or by beginning from the overdoped conventional metallic state. Our view, on the contrary, is that since there is no discontinuous change with doping in the properties of the lamellar copper oxides starting form the antiferromag-

netic insulating state, one will need to understand the evolution from this state of the magnetism and transport as a function of carrier density in order to understand the superconductivity. Even if this is not the case, the approach is a systematic one, which has already led to new and important physics.

High-temperature superconductivity was first discovered by Bednorz and Müller in the material La_2CuO_4 doped with Ba (Bednorz and Müller, 1986). A few months later it was found that doping with Sr raised the superconducting critical temperature T_c in this material to near 40 K, and soon other materials with much higher critical temperatures were discovered. The single common feature of these materials is the two-dimensional CuO_2 layer, and it seems evident that the mechanism of the new superconductivity can be found in the physics of this layer. Whereas the structure of La_2CuO_4 is quite simple, those of the higher-T_c compounds are typically intricate. The $YBa_2Cu_3O_7$ material, for example, with $T_c \sim 90$ K, has chains of alternating Cu and O atoms as well as double CuO_2 layers, and most of the Tl and Bi compounds, with T_c as high as 120 K, have even more complicated structures. It has proven easier to grow large homogeneous single crystals of materials such as La_2CuO_4, $NdCuO_4$, or $Sr_2CuO_2Cl_2$ than of the higher-T_c materials, perhaps because of their relatively simple crystal structure. It appears, therefore, that to understand the physics of the new superconductivity, the simpler materials have advantages.

Since La always has oxidation state + 3 and oxygen has − 2, the chemical composition leads one to conclude that the Cu in La_2CuO_4 is in the + 2 oxidation state, so that its electronic configuration is $3d^9$. With one hole per copper atom one would naively expect La_2CuO_4 to be a metal, and many band-structure calculations have made this expectation quantitative. However, La_2CuO_4 is in fact an antiferromagnetic insulator. This demonstrates dramatically the importance of electron-electron correlations in the copper oxides. Because of these correlations, the holes are localized on the copper atoms.

When La_2CuO_4 is doped for example with Sr, several phase transitions occur. Figure 1 gives the phase diagram of $La_{2-x}Sr_xCuO_4$. The Cu^{2+} spins in undoped La_2CuO_4 order antiferromagnetically with a Néel temperature T_N of approximately 325 K. However, the substitution of Sr^{2+} for La^{3+} introduces holes in the CuO_2 layers, reducing T_N dramatically, as illustrated in Fig. 1. Above about $x = 0.02$, the long-range magnetic order is completely destroyed, but two-dimensional (2D) short-range antiferromagnetic correlations persist. In the antiferromagnet, the transport properties are those of a doped semiconductor, although optical and transport experiments show that the charge carriers are actually polarons. Above about 2% doping, the system behaves like a 2D disordered metal with a gradual crossover from metallic behavior ($dR/dT > 0$) at high T to insulating behavior ($dR/dT < 0$) at low T. Superconductivity appears above about 5% Sr, with T_c reaching $\sim$ 40 K at 15%. The phase boundary for the transition from the orthorhombic to the tetragonal structure is also shown.

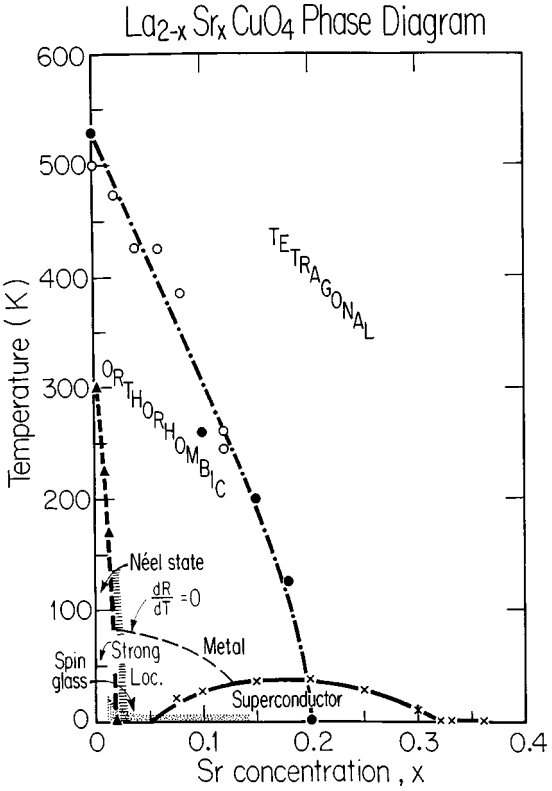

FIG. 1. Phase diagram for $La_{2-x}Sr_xCuO_4$ summarizing structural, magnetic, and transport properties. The narrow dashed line ($dR/dT = 0$) separates the region of metallic linear resistance from that of logarithmically increasing resistance. The conductance in the Néel state is strongly localized. From Keimer, Belk *et al.*, 1992.

An alternative method of doping La_2CuO_4 is to intercalate O^{2-} electrochemically. The excess O^{2-} ions occupy interstitial sites between the CuO_2 layers. Recent work (Wells *et al.*, 1996) has shown that the phase diagram for La_2CuO_{4+y} is quite elaborate, exhibiting phase separation and staging. All of the staged compounds are superconducting, with critical temperatures varying from $\sim$ 31 K for stage 6 to as high as 45 K for the lowest-stage materials. Work on the La_2CuO_{4+y} system is still at an early stage so we will not review it explicitly here.

There have been many reviews of specific aspects, such as optical or transport properties, of the high-T_c superconductors and their semiconducting precursors. The purpose of this paper is to discuss the interrelation of the evolution of transport, optical, and magnetic properties as charge carriers are added to the CuO_2 layers beginning from the undoped insulator. The primary focus is on the pure and lightly doped CuO_2-layer materials. However, we briefly discuss the magnetism in the superconducting phase, as well. We rely heavily on the results of our own experiments on single crystals, but we compare our results with those of other groups, and we discuss results on related materials and ceramics to illustrate the generality of various properties. Reviews of most subjects begin with an apology to those whose work is overlooked. However, in no field of science is it more difficult to be aware of all important contributions

than in the field of high-T_c superconductivity. We hope that our colleagues will understand that our failure to recognize their achievements is the result of our inability to read everything that may be important on this subject.

The organization of this paper is as follows: In Sec. II we briefly summarize the techniques used for growing the large single crystals needed for neutron, transport, and optical measurements. Section III provides an overview of the tetragonal to orthorhombic transition in La_2CuO_4, which, while intrinsically interesting, is especially important because its temperature dependence is very sensitive to the chemical homogeneity of the crystals. Next, in Sec. IV, we discuss the magnetism of undoped La_2CuO_4 and $Sr_2CuO_2Cl_2$, which is well described by the 2D $S = 1/2$ Heisenberg model. Section V reviews the experimental results showing that holes introduced by doping or by photoexcitation form polarons. Recent photoemission measurements indicate that the coupling of a hole to the magnetic fluctuations is critical in determining the band structure, resulting in a band width similar in magnitude to the antiferromagnetic exchange energy. However, the mass of holes near the top of the valence band remains relatively small. The optical measurements reviewed in Sec. V show that the holes are, in addition, dressed by phonons. In Sec. VI we review the evidence that, for light doping, La_2CuO_4 behaves like a conventional doped semiconductor. In Sec. VI we also examine the electronic transport properties near the transition from semiconductor to 2D metal. Then, in Sec. VII, we show how the magnetism evolves with the addition of charge carriers. Conclusions and a summary of outstanding problems is given in Sec. VIII.

II. CRYSTAL GROWTH

Large single crystals of $La_{2-x}Sr_xCuO_4$ have been grown by two techniques. The more common method is solution growth (Hidaka *et al.*, 1987), in which one prepares a melt containing the composition desired as well as excess CuO. The CuO serves as what crystal growers call a flux. This has two functions. First, it lowers the melting point so that crystals can be grown at reasonable temperatures. Typically, the melt must nonetheless be heated to 1300 °C to dissolve the constituents, and the crystals grow upon cooling to $\sim$ 1100 °C. Second, for some materials, like La_2CuO_4, the crystal cannot be grown from the stoichiometric melt, and the flux is essential. This is often called incongruent melting.

Crystals may be grown from the CuO-rich solution using a seed (Picone *et al.*, 1988) or using spontaneous nucleation, as in the technique of Hidaka (Hidaka *et al.*, 1987). In either case, however, one must use a crucible, most commonly made of Pt. Although the amount of Pt incorporated from the crucible in undoped La_2CuO_4 appears to be small, the crucible apparently reacts more rapidly with the SrO and BaO used for doping. Therefore, whereas one can grow crystals of undoped La_2CuO_4 that are relatively pure this way, Pt is sometimes incorporated into the doped crystals at levels of order 1%, which is known to suppress the superconducting T_c.

The second technique avoids contamination by growing the crystals without a crucible. In this traveling-solvent-floating-zone method (Tanaka and Kojima, 1989), a ceramic rod of the appropriate composition is prepared and joined to a second rod containing excess CuO. The latter supplies the solvent (CuO) required for maintaining the proper growth conditions. Then, using high-intensity light, a small region of the rod is melted and this molten region is moved slowly along the length of the rod. With great care and skill, a large crystal can be grown at the boundary of the molten region. In this way single crystals of $La_{2-x}Sr_xCuO_4$ with volumes as large as $\sim$ 1 cm^3 have been grown with $T_c = 38$ K (Hosoya *et al.*, 1992). The critical temperature T_c for crystals grown from Pt crucibles is typically less than $\sim$20 K.

For some materials, crystals may be grown by slow cooling of the stochiometric melt. Figure 2 shows crystals with volumes of order cm^3 grown in the Center for Materials Science and Engineering at MIT by slow cooling, by the top-seeded solution method, and by the traveling-solvent-floating-zone method. Figure 3 is a photograph of the molten region of the rod in the traveling-solvent-floating-zone method.

Because the concentration of Sr in the crystal is, in general, less than that in the melt from which it is grown, special steps must be taken to determine the Sr content. Direct measurements can be made using electron microprobe analysis. In addition, the lattice constants and tetragonal-to-orthorhombic transition temperature, discussed in Sec. III, vary with x, so that these quantities can be used to determine x. Another problem with this technique is that as-grown crystals usually have a dopant-rich layer at the surface. This is not a problem for neutron experiments because the layer is very thin—typically micrometers thick—and thus makes a negligible contribution to experiments that probe the bulk. However, this highly conducting layer can dominate transport and optical measurements, and electron microprobe analysis on as-grown surfaces can be misleading. For optical and transport measurements, samples must be polished and then etched to remove the structural damage induced by polishing. Etching a polished surface for about 10 min in a solution of 1% Br in methanol removes about 1 μm and yields surfaces that are free of etch pits, have excellent optical properties (Falck *et al.*, 1992), and have the same composition as the bulk.

As mentioned previously, the oxygen content can also be varied using electrochemical techniques so that one has the general formula $La_{2-x}Sr_xCuO_{4+y}$. To date, systematic studies varying both x and y have been quite limited.

III. STRUCTURAL PHASE TRANSITIONS AND CHEMICAL HOMOGENEITY

A. Tetragonal-to-Orthorhombic transition in La_2CuO_4

The tetragonal-to-orthorhombic (T-O) transition had been studied (Grande *et al.*, 1977) a decade before the

FIG. 2. (Color) Crystals grown by several methods at MIT. Upper left: Large platelike crystal of Pr_2CuO_4 grown by the top-seeded solution method. Lower left: Top-seeded-solution-grown $La_{1.92}Sr_{0.08}CuO_4$. Top right: $Sr_2Cu_3O_4Cl_2$ grown by slow cooling of the melt. (This novel material is not discussed in this review.) Middle: three rod-shaped crystals of La_2CuO_4 grown by the traveling-solvent-floating-zone method. Middle right: rod-shaped crystal of $La_{1.92}Sr_{0.08}CuO_4$ grown by the traveling-solvent-floating-zone technique. The chip carrier in the lower right, about 2 cm wide, is shown to provide a size scale. Photograph by Felice Frankel.

discovery of high-T_c superconductivity. Soon after the latter discovery it was suggested that the orthorhombic distortion might be driven by strong electron-phonon coupling and might, therefore, be responsible for the insulating state in pure La_2CuO_4, which cannot be explained by band structure. It was furthermore proposed that the same strong electron-phonon coupling might also generate the superconductivity. It is now clear, however, that the distortion has the wrong symmetry to couple strongly to the charge carriers. The phase change is, however, a beautiful example of a soft-phonon-driven structural phase transition (Birgeneau *et al.*, 1987; Böni *et al.*, 1988). Consider, first, the case of pure La_2CuO_4, for which the crystal and magnetic structures are shown in Fig. 4. At high temperatures this material has the same tetragonal structure as K_2NiF_4, space group I4/mmm. Below the temperature T_0, which is about 530 K for undoped La_2CuO_4, the structure transforms to one with orthorhombic symmetry, space group Bmab, because of a staggered tilt of the CuO_6 octahedra, one of which is illustrated in Fig. 4. (Note that in many of our early papers we used the Cmac space group in which the **b** axis, not the **c** axis, is perpendicular to the CuO_2 layers in the orthorhombic structure.) The room-temperature lattice constants of La_2CuO_4 are $a=5.354$ Å, $b=5.401$ Å, and $c=13.153$ Å. Note that the tetragonal cell is drawn in Fig. 4; the orthorhombic cell has lattice vectors in the CuO_2 layer that are the diagonals of the tetragonal cell. The tilt angle of the octahedra, about 4°, is uniform in a given b-c plane. Since there are two equivalent tilt directions in a single CuO_2 layer, crystals are twinned when cooled through the transition in the absence of

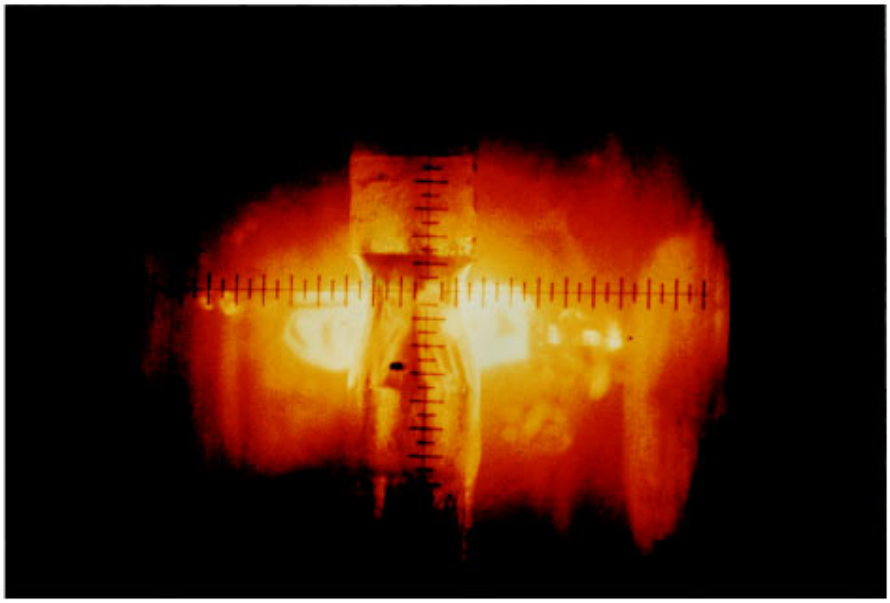

FIG. 3. (Color) Photograph taken during traveling-solvent-floating-zone growth of $La_{2-x}Sr_xCuO_4$ at Tohoku University. The molten zone is narrower than the feed rods.

uniaxial stress. Thio *et al.* (1990) were successful in making a single-domain crystal by cooling through T_0 with a small stress applied along an a axis.

Because of the two equivalent tilt directions, the atomic displacements involved in the transformation from the tetragonal to orthorhombic phase are described by a doubly degenerate order parameter $\{Q_x\} = (Q_\alpha, Q_\beta)$ with wave vectors $\mathbf{q}_\alpha = (1/2,1/2,0)$ and $\mathbf{q}_\beta = (1/2, -1/2,0)$, respectively (Böni *et al.*, 1988). Below T_0, therefore, superlattice reflections $(h/2,k/2,l)$ grow with decreasing T, and the intensities of such peaks scale with the square of the order parameter. Using Landau theory, one also expects the orthorhombic strain, b-a, to be proportional to the square of the order parameter or, equivalently, to scale linearly with the superlattice intensity.

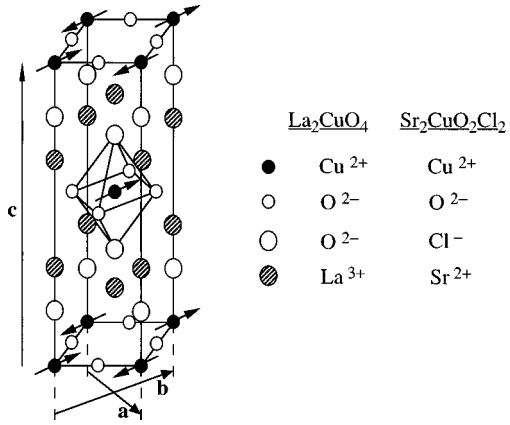

FIG. 4. Crystal and magnetic structure of La_2CuO_4 and $Sr_2CuO_2Cl_2$. The small arrows indicate the arrangement of Cu spins in the Néel state. The elongated octahedron of oxygen ions is drawn for the Cu at the body center. The rotation of this octahedron gives rise to the orthorhombic phase in which a and b are no longer equal.

Figure 5 (Birgeneau *et al.*, 1987) shows the superlattice peak intensity, from neutron measurements, and the strain from x-ray measurements, which follow a power law $(T_0 - T)^{2\beta}$ with $\beta \simeq 0.28$. As discussed in detail by Böni *et al.*, (1988) the symmetries of the Hamiltonian are the same as those of the $3D$, $n = 2$, XY model with cubic anisotropy, for which β is predicted to be 0.35. The disagreement between the theoretical and experimental exponents is probably the result of the small size of the asymptotic critical region.

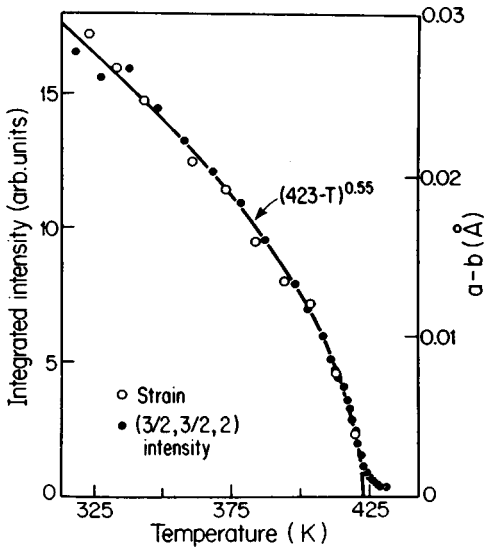

FIG. 5. Neutron-scattering measurement of the intensity of the (3/2, 3/2, 2) superlattice peak, which appears when the crystal acquires orthorhombic symmetry. Also shown is the orthorhombic strain a-b, measured with x rays on a separate crystal from the same boule. The vertical axes have been adjusted to agree on average. The solid line is the best fit to a power law. This boule contained some Li from the flux in which it was grown. From Birgeneau *et al.* (1987).

Studies of the phonon dispersion relations show that the tetragonal-to-orthorhombic transition is driven by the condensing of one of the two zone-boundary (X-point) phonons. The second, uncondensed, mode has relatively low energy ($\sim$ 4 meV) and softens somewhat as T is decreased. Whereas the latter mode does not condense even at very low temperature in pure La_2CuO_4, it does so in $La_{2-x}Ba_xCuO_4$ (Axe *et al.*, 1989; Sera *et al.*, 1989; Yamada *et al.*, 1989) and $(La_{1-z}Nd_z)_{2-x}Sr_xCuO_4$ (Crawford *et al.*, 1991; Keimer *et al.*, 1993). This gives rise to new phases with doubled unit cells, one of which is called the low-temperature tetragonal phase, in which the CuO_6 octahedra rotate about alternate orthogonal axes in successive layers.

Several authors (Ganguly and Rao, 1984; Bringley *et al.*, 1990; Goodenough and Manthiram, 1990) provide compelling evidence that the underlying interaction that gives rise to the low-temperature structural phases is the mismatch in preferred lattice constants of the CuO_2 layer and the intervening rare-earth oxide layers. The CuO_2 layer in La_2CuO_4 is under compressive stress, which leads to the Bmab structure. Replacing La with Nd increases this stress, resulting in the low-temperature tetragonal phase. At high enough Nd concentration the structure changes to the body-centered tetragonal Nd_2CuO_4 phase, similar to the K_2NiF_4 structure, but in which the structure of the rare-earth oxide layer is quite different and the CuO_2 layer is under tension instead of compression. Adding Sr to La_2CuO_4 reduces the compressive stress, both because Sr^{2+} is larger than La^{3+} and because the equilibrium lattice constant of the CuO_2 layer is reduced when its charge becomes less negative. This explains the reduction in the T-O transition temperature with increasing Sr concentration. The reduction in stress is thought to be the driving force for the facility of Sr doping as well as for doping by interstitial oxygen.

B. Strontium and oxygen homogeneity

The crystal used for the measurements of Fig. 5 was grown from a flux containing Li prior to the discovery that Li replaces Cu in La_2CuO_4. The 5% Li in that crystal suppresses T_0 by about 75 K and also eliminates the antiferromagnetic long-range order. The T-O transition is sensitive to Sr composition as well, as can be seen from Fig. 6, which shows superlattice peak intensities for crystals with 0%, 8%, and 14% Sr replacing La (Thurston, Birgeneau, Gabbe, *et al.*, 1989). Because of this, inhomogeneity in the Sr composition leads to rounding of the transition; inhomogeneity of the oxygen concentration has the same effect. From the small rounding of the tetragonal-to-orthorhombic transition, Thurston, Birgeneau, Gabbe, *et al.* (1989) showed that the variation in strontium and oxygen content over the macroscopic dimensions of the crystals of Fig. 6 is less than 0.01 of the Cu atom density. This means that the samples are chemically homogeneous on large length scales, comparable to the size of the entire crystal, which is typically centimeters. Crystals grown more recently

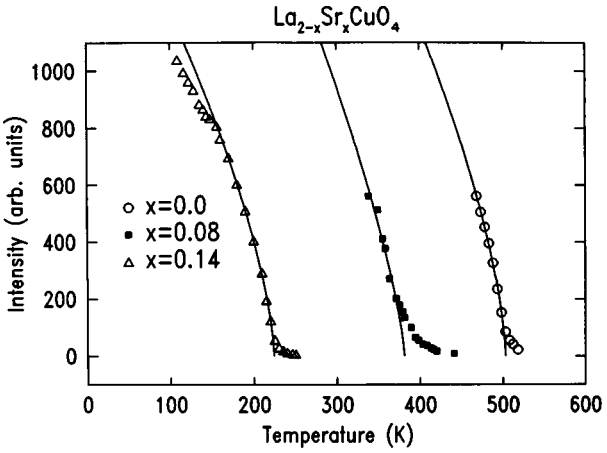

FIG. 6. Superlattice peak intensities in $La_{2-x}Sr_xCuO_4$. The solid lines represent the power law $I = I_0(T_0 - T)^{2\beta}$. The best-fit values of β for the lines shown are 0.33, 0.37, and 0.34 for $x = 0$, 0.08, and 0.14, respectively. From Thurston, Birgeneau, Gabbe, *et al.* (1989).

using the traveling-solvent-floating-zone technique are homogeneous at a level of 0.0006.

In addition, the observation of critical behavior (Fig. 5) implies that the crystals are homogeneous on shorter length scales as well. Böni *et al.* (1988) measured the critical scattering in the crystal MIT-1 (the same one as in Fig. 5) and found that the exponent $\nu = 0.53$ for the inverse correlation length. Using this one infers that, since critical behavior in the order parameter is observed for the doped crystals for reduced temperatures in the range $\sim$ 10% to 1%, and since the rounding of T_0 due to impurity-induced random-field effects is less than 1%, the samples must be homogeneous in a statistical sense down to length scales of $\sim 3 - 10$ lattice constants.

Yamada *et al.* (1995) used the temperature dependence of the T-O transition to show that a large superconducting single crystal is very homogeneous. However, although well-annealed crystals are very homogeneous, rapid thermal cycling can give rise to inhomogeneous oxygen distributions. Thurston and coworkers (Thurston, Birgeneau, Gabbe, *et al.*, 1989; Thurston, Birgeneau, Kastner, *et al.*, 1989) noted that this inhomogeneity could be observed in the rounding of the tetragonal-to-orthorhombic transition and also in shielding measurements on superconducting crystals.

Magnetic susceptibility measurements in the antiferromagnetic phase provide an independent probe of the carrier concentration and homogeneity. As shown in Fig. 1, the Néel temperature is very sensitive to Sr concentration. Chen *et al.* (1995) demonstrated that oxygen-doped and Sr-doped crystals with the same T_N have the same hole density. For crystals of La_2CuO_{4+y} containing no Sr and with oxygen excess y less than $\sim$ 0.01, Preyer, Birgeneau, Chen *et al.*, (1989) showed that the oxygen content is homogeneous to $\Delta y \sim 0.001$. The observation that phase separation occurs on time scales of minutes at relatively low temperatures $\sim$ 200 K for oxygen concen-

trations $y > 0.02$ in La_2CuO_{4+y} indicates that oxygen diffuses rapidly (Jorgensen *et al.*, 1988). Since Preyer *et al.*, saw no evidence of this phase separation for $y \lesssim 0.01$, the oxygen must be uniformly dispersed.

We conclude from studies of the T-O transition, the susceptibility, and shielding measurements that the single crystals are quite homogeneous when annealed for a relatively short period of time to allow the oxygen to diffuse. It appears that it is more difficult to prepare homogeneous ceramics (Harshman *et al.*, 1989).

IV. MAGNETISM IN MATERIALS CONTAINING CuO_2 LAYERS

The discovery of high-temperature superconductivity in 1986 (Bednorz and Müller, 1986) led to a renaissance not only in the field of superconductivity but also in the study of low-dimensional quantum magnetism. The reason for the latter is that the parent compounds such as La_2CuO_4 have magnetic properties that correspond rather well to those of the $S = 1/2$ 2D square lattice quantum heisenberg antiferromagnet (2DSLQHA). Prior to 1986, this 2D quantum spin system represented one of the major unsolved problems in quantum statistical physics. As a result of symbiotic interactions between neutron scattering experiments (Birgeneau *et al.*, 1995; Greven *et al.*, 1995), theory (Chakravarty *et al.*, 1988; Chakravarty *et al.*, 1989; Hasenfratz and Niedermayer, 1991), and Monte Carlo simulations (Ding and Makivic, 1990; Makivic and Ding, 1991), a coherent picture has emerged for the low-temperature properties of the $S = 1/2$ 2DSLQHA. It is now generally agreed that the spin-spin correlation length for the model system diverges exponentially in $1/T$ leading to true long-range order only at $T = 0$. Furthermore, as we review here, the correlation lengths in La_2CuO_4 and $Sr_2CuO_2Cl_2$ are predicted quite well in absolute units by theory.

Soon after the determination by Vaknin *et al.* (1987) of the spin arrangement in the Néel state of La_2CuO_4 shown in Fig. 4, Shirane *et al.* (1987) reported surprising behavior of the spin correlations in the paramagnetic phase. It was found that the spins were correlated over very large length scales at temperatures well above T_N, and that the correlations were perfectly two dimensional. We now understand that the large correlation lengths are a consequence of the large nearest-neighbor Heisenberg exchange energy of ~ 0.13 eV and the two dimensionality of the magnetism.

A direct measure of the large exchange energy comes from two-magnon Raman scattering (Lyons, Fleury, Schneemeyer, and Waszczak, 1988; Lyons, Fleury, Remeika, *et al.*, 1988; Lyons *et al.*, 1989; Sugai *et al.*, 1989; Sugai and Sato, 1989; Sugai *et al.*, 1990). Figure 7 shows the Raman spectra from Tokura *et al.* (1990) for five materials each of which contains isolated CuO_2 layers. The value of J is extracted from data like these using the analysis of the line shape from Singh *et al.* (1989). However, the large width of the two-magnon band is still not completely understood.

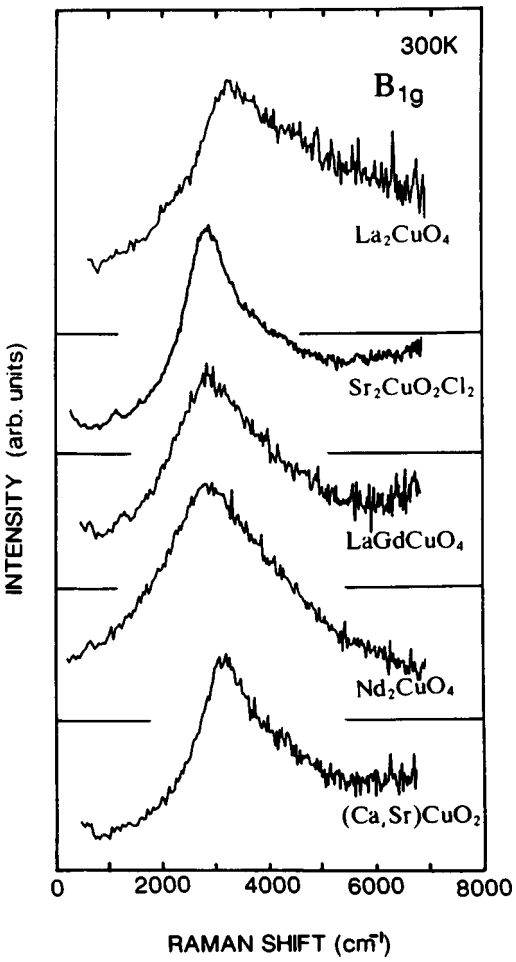

FIG. 7. Raman spectra for two-magnon excitations (B_{1g} symmetry) in five crystals, each containing isolated CuO_2 layers. From Tokura *et al.* (1990).

A variety of experiments have confirmed that the Cu spin system in the CuO_2 layer is a close realization of the $S = 1/2$ 2DSLQHA model. In order to understand most of these experiments, it is necessary to appreciate what is measured in magnetic neutron-scattering experiments, so we discuss this topic first. After these preliminaries, we review the current knowledge of the Néel state, the paramagnetic state, and the transition between them.

A. Magnetic neutron scattering

In all neutron experiments, monochromatized neutrons with initial energy E_i and momentum $\mathbf{k}_i$ are scattered from the sample into a state with final energy $\mathbf{E}_f$ and momentum $\mathbf{k}_f$. Each scattering event is characterized, therefore, by the momentum $\mathbf{Q} = \mathbf{k}_f - \mathbf{k}_i$ and the energy $\hbar\omega$ transferred to the sample. In general, the cross section for scattering of the neutrons by electron spins is given by (Marshall and Lowde, 1968)

$$\frac{\partial^2\sigma}{\partial\Omega_f \partial E_f} \sim |f(\mathbf{Q})|^2 \frac{|\mathbf{k}_f|}{|\mathbf{k}_i|} \sum_{\alpha\beta} (\delta_{\alpha\beta} - \hat{\mathbf{Q}}_\alpha \hat{\mathbf{Q}}_\beta) S^{\alpha\beta}(\mathbf{Q},\omega), \tag{4.1}$$

where

$$S^{\alpha\beta}(\mathbf{Q},\omega)=\frac{1}{2\pi}\int_{-\infty}^{+\infty}dt\sum_{\mathbf{R}}e^{i(\mathbf{Q}\cdot\mathbf{R}-\omega t)}\langle(S^{\alpha}(0,0)S^{\beta}(\mathbf{R},t)\rangle. \tag{4.2}$$

Here, α and β refer to the components of the spin polarization vector. The magnetic form factor $f(\mathbf{Q})$ of Cu^{2+} in La_2CuO_4 has been found to be rather weakly $\mathbf{Q}$ dependent along Q_z, perpendicular to the CuO_2 planes (Freltoft *et al.*, 1988). The quantity $S^{\alpha\beta}(\mathbf{Q},\omega)$ is the dynamic structure factor, the Fourier transform in both space and time of the spin-spin correlation function. For a system with long-range order, Eq. (4.1) for $\omega = 0$ gives the magnetic Bragg scattering:

$$\left.\frac{\partial^2\sigma}{\partial\Omega_f\partial E_f}\right|_{\text{Bragg}}=\sum_{\alpha}(1-\hat{\mathbf{G}}_{\alpha}^2)\frac{1}{N}\langle(S^{\alpha}(\mathbf{G},t)\rangle^2\delta(\omega). \tag{4.3}$$

The directional term $(1 - \hat{\mathbf{G}}^2)$ enables one to determine the ordered spin direction.

The quantity usually predicted by theory is the generalized susceptibility $\chi(\mathbf{Q},\omega)$, whose imaginary part is related to the dynamical structure factor according to

$$S(\mathbf{Q},\omega)=\frac{1}{1-e^{-\hbar\omega/kT}}\,\text{Im}\,\chi(\mathbf{Q},\omega). \tag{4.4}$$

In some experiments one measures $S(\mathbf{Q},\omega)$ itself and, because a triple-axis spectrometer is used to monochromatize both the incident and scattered neutrons while scanning the wave vector, such a measurement is called a three-axis scan. However, to learn about the correlations in the paramagnet, one needs to measure the instantaneous correlation function $S(\mathbf{Q})$. To do this requires an experiment in which one integrates over energy at fixed $\mathbf{q}_{2D}$, obtaining, for the α spin polarization,

$$S^{\alpha\alpha}(\mathbf{q}_{2D})=\int d\omega S^{\alpha\alpha}(\mathbf{q}_{2D},\omega)=\frac{1}{N}\langle S^{\alpha}(-\mathbf{q}_{2D},0)S^{\alpha}(\mathbf{q}_{2D},0)\rangle. \tag{4.5}$$

For a single-layer two-dimensional magnetic system it is possible to adjust the orientation of the crystal such that all neutrons that are collected exit perpendicular to the two-dimensional magnetic layers. Details are discussed by Endoh *et al.* (1988). For this special geometry, merely removing the monochromator from the scattered beam gives an integration over the final neutron energies at fixed in-plane momentum $\mathbf{q}_{2D}$. Because the second monochromator is eliminated, this is called a two-axis scan. It is important to recognize that typically one cannot determine the correlation length accurately with a three-axis scan because the integration over energy is much less accurate.

B. Spin Hamiltonian of La_2CuO_4

Measurements of spin-wave excitations and field-induced transitions in the 3D antiferromagnetic state have provided a fairly complete characterization of the spin Hamiltonian in La_2CuO_4. In addition to the large 2D Heisenberg term, there is coupling between spins in neighboring layers, but this is very small because of frustration: inspection of Fig. 4 shows that in the tetragonal phase each spin has two parallel and two equidistant antiparallel spins in each of the two neighboring layers. The orthorhombic distortion lifts this frustration, resulting in a small antiferromagnetic interlayer exchange. Equally important are anisotropies in spin space. In fact, for the related compound $Sr_2CuO_2Cl_2$, which has the K_2NiF_4 structure to the lowest temperatures measured, the interlayer coupling is very weak, and the spin anisotropies are the dominant deviations from the 2D Heisenberg term in the Hamiltonian.

Taking spin-orbit coupling into account, the Hamiltonian has the general form

$$H=\sum_{i\delta}\mathbf{S}_i\cdot\vec{\mathbf{J}}\cdot\mathbf{S}_{i+\delta},$$

where the index i refers to a Cu site and δ to its nearest neighbors, both within and perpendicular to the plane. The spin anisotropies are reflected in the fact that the exchange is a tensor rather than a scalar. In the tetragonal K_2NiF_4 structure $\vec{\mathbf{J}}$ is diagonal with different elements parallel and perpendicular to the layers. However, the rotation of the CuO_6 octahedra around the $\hat{\mathbf{b}}$ direction, leading to the orthorhombic phase in La_2CuO_4, allows an additional off-diagonal spin anisotropy, the Dzyaloshinski-Moriya (DM) antisymmetric exchange (Thio *et al.*, 1988). In general, the Hamiltonian may be written

$$H=J\left(\sum_{i,\delta\|}\vec{\mathbf{S}}_i\cdot\vec{\mathbf{S}}_{i+\delta\|}+\alpha_{xy}\sum_{i,\delta\|}\mathbf{S}_i^c\mathbf{S}_{i+\delta\|}^c+\sum_{i,\delta\perp j}\alpha_{\perp j}\vec{\mathbf{S}}_i\cdot\vec{\mathbf{S}}_{i+\delta\perp j}+\alpha_{DM}\sum_{i,\delta\|}(-)^i\hat{\mathbf{b}}\cdot\mathbf{S}_i\times\mathbf{S}_{i+\delta\|}\right). \tag{4.6}$$

Here, α_{xy}, $\alpha_{\perp j}$, and α_{DM} represent the x-y anisotropy, the interlayer coupling, and the Dzyaloshinski-Moriya term, respectively, and $\mathbf{S}_i^c$ is the $\mathbf{c}$ component of the spin at site i. The third term of Eq. (4.6) explicitly includes the two different out-of-plane neighbors at $\delta_{\perp 1}$ and $\delta_{\perp 2}$. Note that, as was implicit in the work of Thio *et al.* (1988), the sign of the antisymmetric term changes on the opposite sublattices because of the opposite rotation of the octahedra.

Near the center of the Brillouin zone, above the gaps resulting from anisotropy, the spin-wave dispersion relation is linear, $\omega = c|\mathbf{q}_{2D}|$ with spin wave velocity $c = 1.17\sqrt{2}Ja/\hbar$, where a is the Cu-Cu nearest-neighbor distance. The coefficient 1.17 results from quantum renormalization, which is important for spin 1/2. The very large value of J means that epithermal neutrons are required to measure the dispersion relation away from the zone center. Results of such experiments for La_2CuO_4 (Aeppli *et al.*, 1989; Hayden *et al.*, 1991) shown in Fig. 8 are consistent with the conventional theory of the 2D $S = 1/2$ Heisenberg Hamiltonian with J

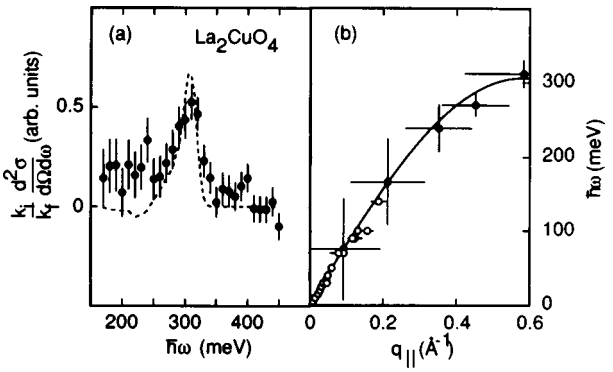

FIG. 8. High-energy spin waves in La_2CuO_4: (a) Neutron-scattering spectrum chosen to emphasize the magnon scattering near the zone boundary, $\mathbf{Q} \approx (1,k,0.5)$. The dashed line is a resolution-corrected nearest-neighbor spin-wave model. (b) The dispersion relation deduced from spectra like that in (a). From Hayden *et al.*, 1991.

$= 135$ meV, the value extracted from two-magnon light-scattering experiments (Lyons *et al.*, 1989; Singh *et al.*, 1989). For $Sr_2CuO_2Cl_2$, the latter experiments give $J = 125$ meV (Tokura *et al.*, 1990).

Because of the x-y anisotropy, there is a gap in the out-of-plane mode of magnitude $2.34J\sqrt{2\alpha_{xy}}$, and because of the antisymmetric exchange [the last term in Eq. (4.6)], in La_2CuO_4 there is an in-plane gap of magnitude $2.34J\alpha_{\mathrm{DM}}$. The values of the anisotropies determined in this way are in agreement with those determined from susceptibility measurements for La_2CuO_4 (Thio and Aharony, 1994), specifically, $\alpha_{xy} = 1.5 \times 10^{-4}$, $\alpha_{\perp j} = 5 \times 10^{-5}$, and $\alpha_{\mathrm{DM}} = 7.5 \times 10^{-3}$ (Keimer, Belk *et al.*, 1992). However, for $Sr_2CuO_2Cl_2$ the largest of these terms α_{DM} is missing. For the latter material spin-wave-gap measurements give $\alpha_{xy} = 1.5 \times 10^{-4}$; $\alpha_{\perp j}$ is too small to measure because of the perfect frustration of the nearest-neighbor interlayer exchange (Greven *et al.*, 1995).

The antisymmetric exchange makes the phase diagram of La_2CuO_4 more elaborate than that of $Sr_2CuO_2Cl_2$. The Dzyaloshinski-Moriya term, because it involves the vector product of neighboring spins, causes the spins of the Cu ions to cant out of the CuO_2 layers by a small angle, about 0.17°. As a result, each layer has a small net moment, about $2 \times 10^{-3}\mu_B$ per Cu atom, in the c direction, normal to the layer. However, the weak interlayer coupling causes the moments of successive layers to order antiferromagnetically, so the weak ferromagnetism is hidden in the Néel state at zero field. When a sufficiently strong magnetic field is applied in the c direction, the coupling of the spins to the external field overcomes the interlayer coupling, and a transition takes place to ferromagnetic ordering of the layers (Thio *et al.*, 1988; Thio and Aharony, 1994). Furthermore, the Dzyaloshinski-Moriya interaction gives rise to the truncated ferromagnetic peak in the susceptibility at T_N. Using a mean-field theory for the interlayer coupling and the renormalized classical susceptibility of the $S = \frac{1}{2}$ 2DSLQHA, discussed below, Thio and Aharony (1994) obtained an excellent fit to the data, as shown in Fig. 9.

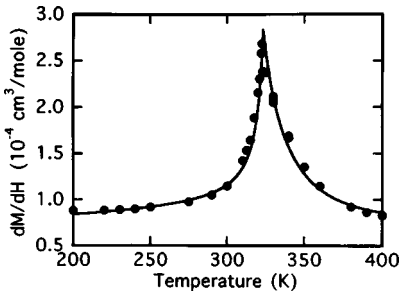

FIG. 9. Magnetic susceptibility $\chi = dM/dH$ for $H \| c$, perpendicular to the CuO_2 layer, for La_2CuO_4. The solid line is a fit to the mean-field theory. From Thio and Aharony (1994).

C. Antiferromagnetic spin correlations in the paramagnetic phase

The first neutron experiments on La_2CuO_4 revealed that, in the paramagnetic phase immediately above T_N, the spins in a given CuO_2 layer are correlated instantaneously over very large distances while spins in adjacent layers are completely uncorrelated. It soon became clear that the large correlation length was the result of both the two dimensionality and the large Heisenberg exchange energy. Indeed, if the spins were classical, the correlation lengths would be much larger than observed. However, when first discovered, the large correlation lengths were a surprise and stimulated a variety of theoretical studies to elucidate the basic static and dynamic spin correlations of the $S = \frac{1}{2}$ 2DSLQHA.

In particular, Chakravarty, Halperin, and Nelson (Chakravarty *et al.*, 1988; Chakravarty *et al.*, 1989) have provided a comprehensive theory of the 2DSLQHA. Their result for the correlation length in the renormalized classical region has been further refined by Hasenfratz and Niedermayer (1991). The result is

$$\xi/a = \frac{e}{8}\frac{\hbar c/a}{2\pi\rho_s}\exp\{2\pi\rho_s/kT\}\left[1-\frac{1}{2}\left(\frac{kT}{2\pi\rho_s}\right)+O\left(\frac{kT}{2\pi\rho_s}\right)^2\right], \tag{4.7}$$

where ρ_s is the spin stiffness constant, and c is the spin-wave velocity. The relationships between c, ρ_s, and J are now accurately known for the $S = \frac{1}{2}$ 2DSLQHA (Beard *et al.*, 1998)—specifically, $\hbar c = 1.657Ja$ and $2\pi\rho_s = 1.131J$. Using these relationships, one then has

$$\xi/a = 0.498\exp\{1.131J/kT\}\left[1-0.44\left(\frac{kT}{J}\right)+O\left(\frac{kT}{J}\right)^2\right], \tag{4.8}$$

in the renormalized classical regime. As is clear from Eq. (4.7) or Eq. (4.8) the temperature dependence of ξ is dominated by the exponential factor and is, therefore, nearly the same as that of the classical 2D Heisenberg antiferromagnet, $\xi \sim \exp(2\pi J/kT)$. The quantum renor-

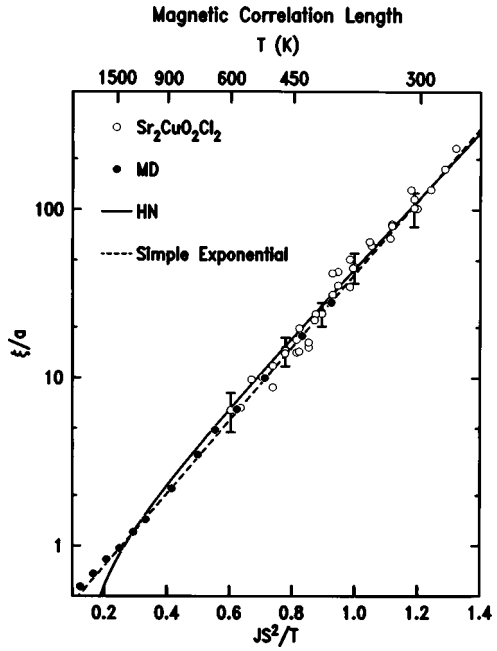

FIG. 10. Semilog plot of the reduced magnetic correlation length ξ/a vs J/T. The open circles are data for $Sr_2CuO_2Cl_2$ using $J = 125$ meV and the measured lattice constant. The filled circles are the results of the Monte Carlo simulations of Makivic and Ding (1991). The solid line is the theoretical prediction of the $S = \frac{1}{2}$ 2D nonlinear sigma model from (Hasenfratz and Niedermayer, 1991). The dashed line is the simple exponential form $\xi/a = 0.276\exp(1.25\,\mathrm{J/kT})$ suggested by Makivic and Ding (1991). From Greven *et al.* (1995).

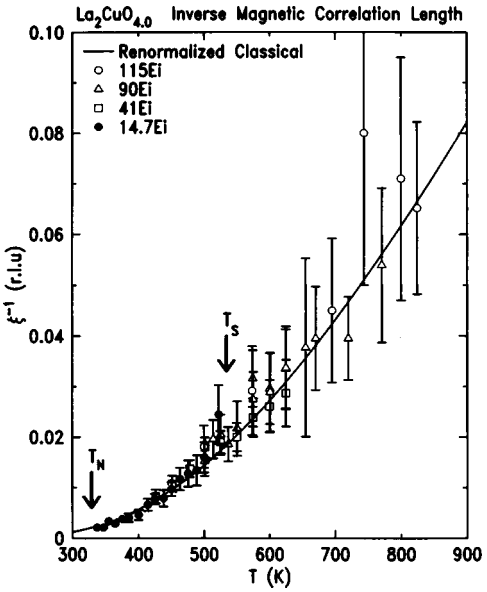

FIG. 11. Inverse magnetic correlation length in La_2CuO_4. The solid line is Eq. (4.7) with $J = 135$ meV. The Néel and structural transition temperatures are indicated by arrows. From Birgeneau *et al.* (1995).

malization of ρ_s makes the correlation length much shorter than the classical value, although it is still very large near T_N.

Figure 10 shows a comparison of the theory with measurements of ξ for $Sr_2CuO_2Cl_2$ (Greven *et al.*, 1994; Greven *et al.*, 1995). The inverse correlation length $\kappa = \xi^{-1}$ is obtained at each temperature from fits of the measured $S(\mathbf{q}_{2D})$ to a Lorentzian, $S(0)/(\kappa^2 + q_{2D}^2)$. The solid curve in Fig. 10 is Eq. (4.7) with $2\pi\rho_s$ fixed at its theoretical value of $1.131J$, where $J = 125$ meV is deduced from two-magnon Raman scattering (Tokura *et al.*, 1990). The Monte Carlo results of Makivic and Ding (1991), also shown in Fig. 10, are well described by the simple form $\xi = 0.276a\ \exp\{1.25\,\mathrm{J/kT}\}$, which agrees with experiment if one chooses $J = 125$ meV. It is important to emphasize that the theory gives the correlation length, in reciprocal lattice units, with no adjustable parameters. This is an impressive achievement.

As for the case of $Sr_2CuO_2Cl_2$, first-generation experiments on La_2CuO_4 by Keimer, Belk, *et al.* (1992) had shown good agreement with Eq. (4.8), although there appeared to be some systematic discrepancy for high temperature at the limits of the error bars. More importantly, NMR measurements by Imai *et al.* (1993) had suggested that for $T > 600$ K there was a crossover from the renormalized classical behavior of Eq. (4.7) to quantum critical behavior ($\xi \sim 1/T$).

In order to elucidate this possible crossover, Birgeneau *et al.* (1995) extended the measurements of Keimer *et al.* (Keimer, Belk, *et al.*, 1992) to both lower and higher temperatures. To guarantee complete integration over all important dynamical fluctuations they used progressively higher incoming neutron energies at higher temperatures and hence shorter correlation lengths. Their results are shown in Fig. 11. The spin-wave velocity $\hbar c = 850$ meV Å, and hence $J = 135$ meV, are known from inelastic neutron-scattering measurements (Aeppli *et al.*, 1989; Hayden *et al.*, 1991)—see Fig. 8. The solid line in Fig. 11 is Eq. (4.7) with $J = 135$ meV. Clearly the agreement between the theory of Chakravarty *et al.* (1988, 1989) and of Hasenfratz and Niedermayer (1991) for the 2D quantum nonlinear sigma model and the Birgeneau *et al.* data in La_2CuO_4 (Birgeneau *et al.*, 1995) is excellent, as it is for $Sr_2CuO_2Cl_2$. There is, in addition, no evidence for the predicted crossover from renormalized classical to quantum critical behavior for $T > 600$ K (Chubukov and Sachdev, 1993; Imai *et al.*, 1993; Sokol *et al.*, 1994). This excellent agreement with the low-temperature renormalized classical prediction of Eq. (4.7) over such a wide range of energy scales and to such high temperatures must be considered surprising (Elstner *et al.*, 1995). Further, recent measurements in the $S = 1$ system La_2NiO_4 (Nakajima *et al.*, 1995), together with a reanalysis of early measurements in K_2NiF_4 shows that Eq. (4.7) describes the $S = 1$ 2DSLQHA results quite well, but only if ρ_s is reduced by about 20% from its theoretical value. This discrepancy appears quite surprising given the good agreement discussed above of the three-loop theory with experiments for the $S = 1/2$ materials. This issue has recently been addressed by Beard *et al.* (1998)—they have combined an accurate quantum Monte Carlo technique with finite-size scaling for the $S = 1/2$ 2DSLQHA. This has made possible the determination of ξ down to very low

temperatures and hence very large length scales. Their resultant Monte Carlo correlation length data cover the distance range from $\sim 3 \times 10^5$ to 1 lattice constant with increasing temperature. Beard *et al.* (1998) find that the higher-order terms $O(kT/2\pi\rho_s)^2 + \cdots$ in Eq. (4.7) are offset by finite lattice correction effects so that the net deviation from the three-loop result, Eq. (4.7) without the $O(kT/2\pi\rho_s)^2 + \cdots$ higher-order terms, is never more than about 10%, which is within the accuracy of the experiments. Thus the excellent agreement between the three-loop result for the quantum nonlinear sigma model and the experimental plus Monte Carlo data shown in Figs. 10 and 11 is, in part, accidental. Concomitantly, the disagreement of Eq. (4.7) with experimental and numerical data for higher-spin systems most likely originates from the fact that the data are not in the asymptotic scaling regime, as conjectured by Elstner *et al.* (1995).

D. The Néel transition

Beginning in the paramagnetic state at temperatures well above $T = J/k$, temperatures that are inaccessible because $J \sim 1300$ K, one expects the spins to be completely uncorrelated. As the temperature is lowered through $T \sim J/k$, the correlation length grows rapidly, as we have seen, but only within the 2D CuO_2 layer. On the one hand, in a 3D antiferromagnet, long-range order would occur at $T_N \sim J$. On the other hand, if the system were genuinely two dimensional and purely Heisenberg, long-range order would occur only at $T = 0$. Coming from high temperature, the interlayer coupling and anisotropy in spin space become increasingly important as the correlation length grows. The Néel transition occurs when the non-Heisenberg terms in the spin Hamiltonian multiplied by the number of spins in a correlated region is of order kT. In fact, one can estimate the Néel temperature fairly accurately from the simple relation $kT_N = (\xi/a)^2 J\alpha_{\rm eff}$, and $\alpha_{\rm eff} = z_\parallel\alpha_{xy} + z_\perp\alpha_\perp$, where $z_\parallel$ and $z_\perp$ are the in- and out-of-plane coordination numbers, respectively, and ξ is given by Eq. (4.7) or Eq. (4.8). The tetragonal materials, $Sr_2CuO_2Cl_2$, Sm_2CuO_4, and Pr_2CuO_4 have Néel temperatures that are within $\sim 20\%$ of that for La_2CuO_4. Since $\alpha_\perp$ is orders of magnitude smaller in the tetragonal materials because of the perfect frustration of the interlayer exchange, it is clear that α_{xy} plays a dominant role for the tetragonal materials and is important for La_2CuO_4 as well.

In an effort to include both of these effects, Keimer, Aharony, *et al.* (1992) produced a generalization of the Schwinger boson mean-field theory, which provides a simple prediction of the Néel temperature. They show that their numerical results are well described by

$$\frac{kT_N}{J} \approx \frac{M_0\pi}{\log[4\alpha_{\rm eff}/(M_0\pi^2\log(4\alpha_{\rm eff}/\pi))]}, \tag{4.9}$$

where $2M_0 \approx 0.6$ is the $T = 0$ sublattice magnetization. Equation (4.9) is an interpolation formula that reduces to the mean-field criterion $kT_N = J\alpha_{\rm eff}(\xi/a)^2$ given above. For La_2CuO_4 $\alpha_\perp \sim \alpha_{xy}$, and in the tetragonal materials $\alpha_\perp \ll \alpha_{xy}$, since the interlayer Heisenberg coupling is perfectly frustrated. However, since α_{xy} is about the same size in all materials and since T_N depends only logarithmically on $\alpha_{\rm eff}$, one can understand why the Néel temperatures are so similar.

For Ising systems with reduced Ising anisotropy, α_I, the correlation length to leading order is

$$\xi(\alpha_I, T)/a = \frac{\xi_H(T)/a}{\sqrt{1-\alpha_I(\xi_H(T)/a)^2}}, \tag{4.10}$$

where $\xi_H(T)/a$ is given by Eq. (4.7). Thus the Néel temperature is determined by

$$\xi_H(T_N)/a = \sqrt{1/\alpha_I}. \tag{4.11}$$

In K_2NiF_4, which is a quasi-two-dimensional $S = 1$ Ising system, Eq. (4.11) predicts the Néel temperature to within 1% provided that ρ_s is chosen so that Eq. (4.7) properly describes the measured correlation length in the Heisenberg region. Equation (4.10) also properly captures the crossover from 2D Heisenberg to 2D Ising behavior in K_2NiF_4 as well as in La_2NiO_4 (Greven *et al.*, 1995; Nakajima *et al.*, 1995).

In summary, the spin-spin correlation lengths in $Sr_2CuO_2Cl_2$ and La_2CuO_4 agree quantitatively with quantum Monte Carlo simulations for the $S = 1/2$ 2DSLQHA over a wide range of temperature. The combined experimental and Monte Carlo data, which cover the length scale from ~ 1 to 200 lattice constants, are in turn predicted accurately without adjustable parameters by the theory of Chakravarty, Halperin, and Nelson (1988, 1989) and Hasenfratz and Niedermayer (1991) to $O(kT/2\pi\rho_s)^2$. In addition, the transition from the paramagnetic state, with its very long correlation lengths, to the Néel state is fairly well described by mean-field theory. The theory appears to be successful in the $S = 1$ systems K_2NiF_4 and La_2NiO_4 provided that ρ_s is reduced by $\sim 20\%$ from its theoretical value. However, in all of the materials the peak of the static structure factor follows the simple form $S(0) \sim \xi^2$ (Keimer, Belk *et al.*, 1992; Greven *et al.*, 1995) rather than $\sim T^2\xi^2$ as predicted by current theory (Chakravarty *et al.*, 1988; Chakravarty *et al.*, 1989; Kopietz, 1990). Although the latter result is not rigorous, in contrast to the Hasenfratz-Niedermayer result for the correlation length, it appears to be quite universal as it is seen in both $S = 1/2$ and $S = 1$ systems (Greven *et al.*, 1995; Nakajima *et al.*, 1995). This represents an important challenge for the theory of the 2DSLQHA.

V. OPTICAL PROPERTIES OF UNDOPED AND LIGHTLY DOPED CuO_2 LAYERS

Optical studies of electronic excitations have revealed much about the nature of the charge carriers and the neutral excitations, excitons, in materials containing single CuO_2 layers. In this section we first review the optical properties of the undoped compounds, and then turn to some aspects of lightly doped CuO_2 layers. In Sec. V.A we present a discussion of infrared optical ab-

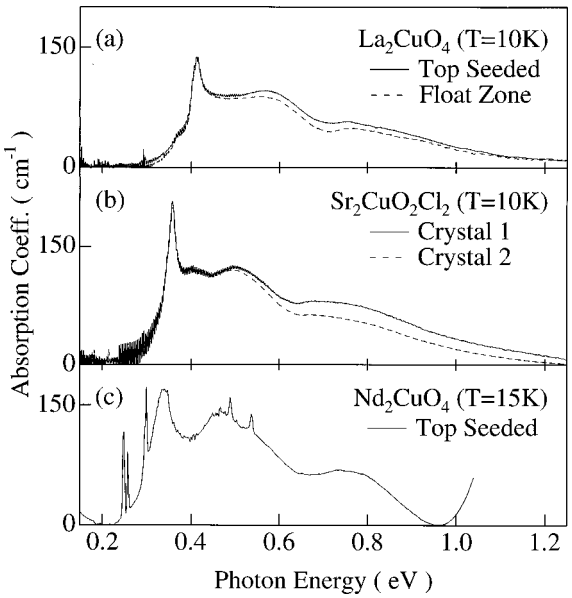

FIG. 12. Absorption coefficient vs photon energy in α polarization (propagation normal to the CuO_2 layers) for single crystals of different composition. For La_2CuO_4, spectra are shown for crystals grown by two techniques and for $Sr_2CuO_2Cl_2$ spectra are shown for two crystals grown with starting materials of different purity. The agreement shows that the absorption is intrinsic. For Nd_2CuO_4 the sharp features result from transitions between f levels. From Perkins *et al.* (1998).

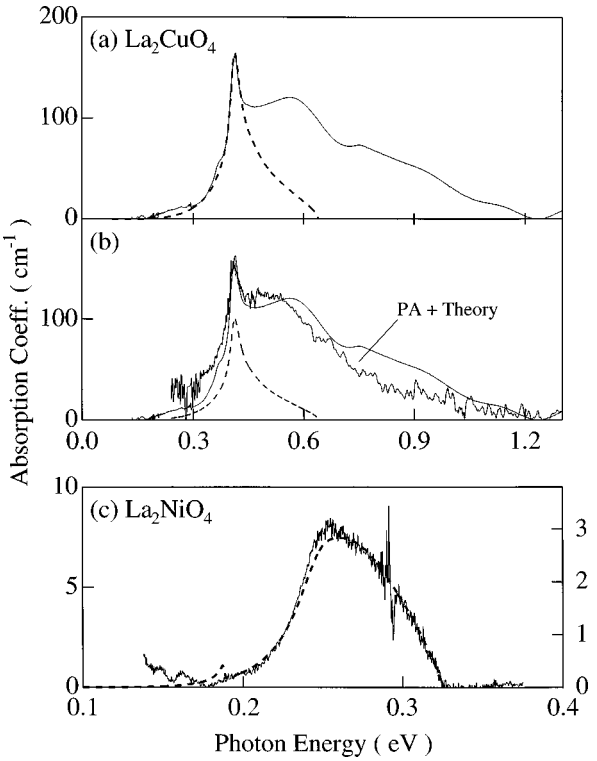

FIG. 13. Comparison of the theoretical predictions (dashed curves) of Lorenzana and Sawatzky (1995a, 1995b) for the optical absorption spectra (a), (b) in carrier-free La_2CuO_4 and (c) La_2NiO_4. For La_2NiO_4 the scale for the theoretical curve is on the left and that for the experiment is on the right. For (a) the theoretical spectrum is multiplied by a factor ~ 4 to match the experiment at the peak. For (b) the curve labeled PA+Theory is obtained by multiplying the theoretical spectrum by 2.4 and adding it to the photoinduced absorption spectrum. From Perkins *et al.* (1998).

sorption in undoped crystals. Some of this absorption results from the creation of Frenkel excitons corresponding to crystal-field excitations of the Cu^{2+} ions. However, recent theoretical and experimental studies provide convincing evidence that part of the absorption corresponds to the creation of bimagnons coupled to phonons. In Sec. V.B we review studies of the charge-transfer excitations, which result in mobile charge carriers. The temperature dependence of the charge-transfer absorption provides strong evidence that the charge carriers are large (Fröhlich) polarons. Section V.C discusses evidence that polaronic effects are even more pronounced for holes bound to impurities than for mobile ones.

A. Mid-infrared absorption in carrier-free materials

Perkins *et al.* (1993) discovered infrared absorption common to all materials containing the CuO_2 layer. Figure 12 shows this weak absorption in single crystals of three materials with single layers, La_2CuO_4, $Sr_2CuO_2Cl_2$, and Nd_2CuO_4. Very similar spectra have been reported for carrier-free Pr_2CuO_4 (Perkins *et al.*, 1993) and $YBa_2Cu_3O_6$. (Grüninger *et al.*, 1996).

Lorenzana and Sawatzky (1995a, 1995b) have argued convincingly that the sharp peak at ~ 0.35 eV results from the creation of a quasibound state of two magnons made weakly allowed by coupling to an optical phonon. They find that the bimagnon state is relatively long lived because the magnon-magnon interaction lowers its energy into a region where the density of states for decay of the two-magnon bound state into other magnons is low. Figures 13(a) and 13(b) show the prediction of Lorenzana and Sawatzky together with the experiments of Perkins *et al.*, (1993) for La_2CuO_4. According to Lorenzana and Sawatzky, the absorption spectrum is dominated by magnon pairs with momentum near $(\pi,0)$. They therefore choose the phonon energy to be that of the in-plane Cu-O stretching mode at $(\pi,0)$. The value of J that they use to fit the peak position is in good agreement with that from two-magnon Raman scattering. The theoretical intensity shown in Fig. 13(a) has been adjusted to match the sharp peak intensity. In Fig. 13(b) we take the background from measurements of photoinduced absorption, as discussed below (Perkins *et al.*, 1998). In this case, the peak is scaled up ~ 2.4 from the Lorenzana-Sawatzky calculation in order to obtain agreement with the measured peak intensity.

The same theory (Lorenzana and Sawatzky, 1995a, 1995b) predicts a very different line shape for La_2NiO_4, which has the same structure as La_2CuO_4, but with Ni ($S = 1$) replacing Cu ($S = 1/2$). Figure 13(c) shows the comparison of theory with experiment (Perkins *et al.*, 1995) for La_2NiO_4 with only the magnitude of the absorption adjusted. The excellent agreement implies that

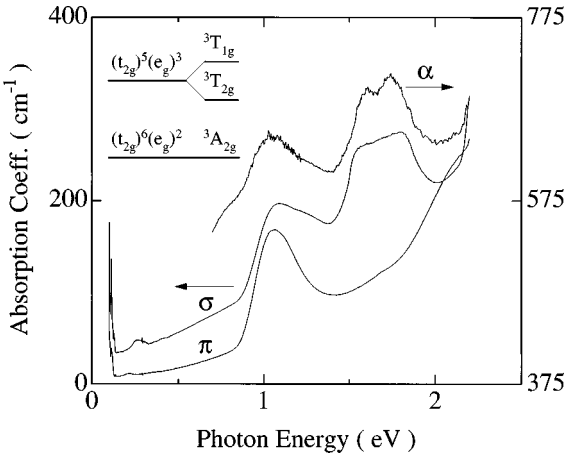

FIG. 14. Absorption coefficient for La_2NiO_4 for the three possible polarizations at 10 K. The σ spectrum has been shifted upward by 20 cm^{-1} and the α spectrum has been shifted downward as indicated by the right-hand scale. The inset shows a level diagram for Ni^{2+} in an octahedral (O_h point group) crystal field. The left part of the level diagram is for noninteracting electrons, whereas the right part is for electron interaction strength comparable to the crystal field. From Perkins *et al.* (1995).

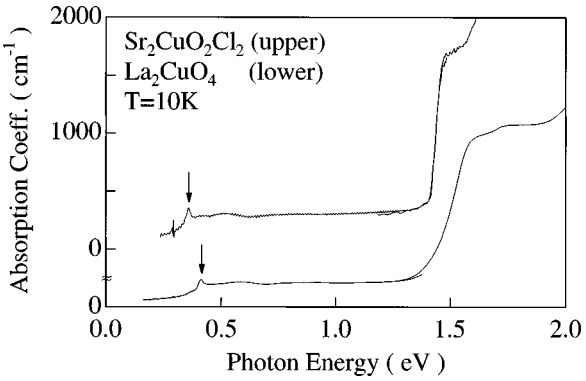

FIG. 15. Absorption coefficient for two materials in α polarization over a larger photon energy range than in Fig. 12. The peaks seen in Fig. 12 are indicated by arrows. The crystal-field excitonic absorption sets in strongly above 1.4 eV. From Perkins *et al.* (1998).

in this case the entire absorption results from the creation of bimagnons plus phonons.

Figure 14 shows the absorption in La_2NiO_4 over a larger energy range (Perkins *et al.*, 1995). The bimagnon absorption, just discussed, is much weaker than the Frenkel excitons seen in the range $\sim 1-2$ eV. Spectra are shown for the three possible polarizations: propagation of light normal to the CuO_2 layers (α), propagation parallel to the layers with electric field parallel to the layers (σ), and propagation parallel to the layers with electric field perpendicular to the layers (π). Large single crystals are necessary for such polarization measurements. The observation of bands in σ and α but not in π show that the excitations are weakly electric dipole allowed, presumably because of coupling to optical phonons. The same polarization properties are observed for the spectra in Fig. 12.

The bands in this spectral range are similar to those in other Ni compounds (Ballhausen, 1962). They arise from excitations between crystal- or ligand-field states that result from the splitting of the Ni ion d levels by the oxygen ligands. The lowest few energy levels are sketched in the inset of Fig. 14 for octahedral coordination of the Ni ion in the strong-field limit, for which the crystal-field potential is much larger than the electron-electron Coulomb interaction, and in the intermediate regime, in which these energies are comparable (Ballhausen, 1962). The latter case is appropriate for Ni^{2+} in La_2NiO_4. Because the two excited $^3T_{2g}$ and $^3T_{1g}$ (O_h notation) states are spin triplets, transitions from the ground $^3A_{2g}$ state are spin allowed. In a tetragonal field, the spatial degeneracy of the $^3T_{1g}$ and $^3T_{2g}$ states is lifted, as seen in the spectra of K_2NiF_4 and Rb_2NiF_4 (Iio and Nagaka, 1976). The latter have the same crystal structure as the high-temperature structure of La_2NiO_4.

Thus for La_2NiO_4, the magnetic- and crystal-field excitations are well separated in energy and fairly easily identified. For La_2CuO_4, however, the situation is more complicated. The theory of Lorenzana and Sawatsky (1995a, 1995b) explains the sharp peak near 0.35 eV, but not the broad absorption between ~ 0.4 and 1.2 eV. Perkins *et al.* (1993) have suggested that this absorption arises from multimagnon sidebands of an electric-dipole forbidden crystal-field exciton at ~ 0.4 eV. In particular, they propose that the Frenkel exciton corresponds to the transition from the x^2-y^2 ground-state orbital of the hole on the Cu^{2+} ion to the $3z^2$-r^2 orbital. On the one hand, the low energy of this excitation is surprising because cluster calculations (McMahan *et al.*, 1988; Eskes *et al.*, 1990; McMahan *et al.*, 1990) generally predict the $d_{3z^2-r^2}$ level to lie about 1 eV above the $d_{x^2-y^2}$ state. On the other hand, several results suggest that the $d_{3z^2-r^2}$ state is indeed at ~ 0.4 eV as argued by Perkins *et al.* (1993).

One indirect piece of evidence is that the other crystal-field excitations are easily seen in optical absorption above 1 eV, but the transition from the x^2-y^2 orbital to the $3z^2$-r^2 orbital is missing. An absorption at ~ 1.5 eV, seen for $Sr_2CuO_2Cl_2$ and La_2CuO_4 in Fig. 15 (Perkins *et al.*, 1993), results from the transition between the x^2-y^2 orbital and the xy orbital, whereas the transitions to the yz and zx orbitals are near 1.6 eV. This has been demonstrated by electroreflectance measurements with applied electric fields normal and perpendicular to the CuO_2 layers, which are sensitive to the symmetry of the transitions (Falck *et al.*, 1994). Raman scattering studies have confirmed this (Liu *et al.*, 1993; Salamon *et al.*, 1995). However, Salamon *et al.* (1995) failed to observe the $3z^2$-r^2 state between 1 and 2 eV. Thus the $3z^2$-r^2 level must be at lower energy than predicted by most cluster calculations.

In addition, Bianconi *et al.* (1987) used polarized x-ray absorption spectroscopy to put an upper limit on the $d_{x^2-y^2} - d_{3z^2-r^2}$ splitting of ~ 0.5 eV. This interpretation is supported by calculations that imply that a small $d_{x^2-y^2}$-$d_{3z^2-r^2}$ splitting is required to account for the Cu

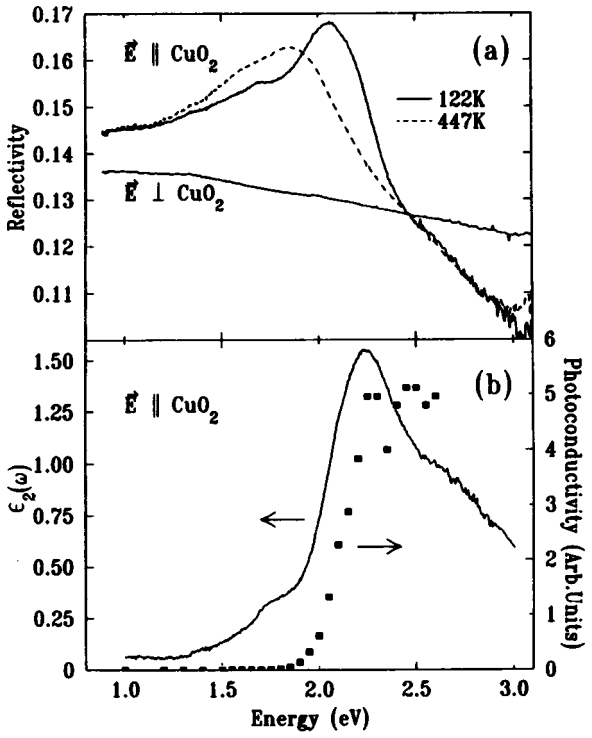

FIG. 16. Spectra of La_2CuO_4: (a) Reflectivity at two temperatures with the electric field in the plane of the CuO_2 layer and at one temperature with the field perpendicular to the layer for comparison. (b) In-plane $\varepsilon_2(\omega)$ at $T = 122$ K together with the photoconductivity at $T = 132$ K for an identically-prepared single crystal. From Thio, Birgeneau, *et al.* (1990) and Falck *et al.* (1992).

$d_{3z^2-r^2}$ character of the doped holes (Grilli *et al.*, 1990).

When carriers are added by doping or by photoexcitation, the broad sidebands between ~ 0.4 and ~ 1 eV grow dramatically, whereas the sharp peak does not (Perkins *et al.*, 1998). This is our motivation for adding the photoinduced absorption spectrum to the theoretical spectrum of Lorenzana and Sawatsky (1995a, 1995b) for comparison with experiment in Fig. 13. This is further evidence that the two components have different microscopic origins. The broad midinfrared absorption, which appears to result from an intensification and broadening of the intrinsic bands seen in Fig. 12, is a common feature of the high-T_c materials and has been discussed by many authors (Thomas, 1991). However, most authors ascribe this absorption to other electronic origins.

B. Charge-transfer excitations

In La_2CuO_4, the excitonic absorption extends up to about 2 eV. However, above 2 eV the dominant absorption gives rise to charged rather than neutral excitations. Figure 16 shows the reflectivity together with the imaginary part of the dielectric function ε_2 derived from Kramers-Kronig transformation of the reflectivity (Falck *et al.*, 1992). The absorption is completely polarized with the electric-field vector in the CuO_2 layer. Also shown are measurements of the photoconductivity (Thio *et al.*, 1990). The comparison of these two measurements shows that the absorption above 2 eV gives rise to charged excitations that contribute to the conductivity, whereas absorption at lower energies does not.

The peak in ε_2 near 2.2 eV has been explained by Falck *et al.* (1992). For noninteracting electron-hole pairs, the absorption spectrum would be a step function at the gap, because of the constant density of states for the two-dimensional electron states in the CuO_2 layer. However, the electron-hole interaction modifies the spectrum dramatically. Falck *et al.* (1992) assume a short-range interaction between electron and hole, appropriate for a system with Frenkel excitons. Using a delta-function interaction $V(\mathbf{r}) = -g\,\delta(\mathbf{r})$, the problem can be solved exactly and yields

$$\varepsilon_2(\omega) = \frac{\mathrm{Im}\ F(\omega)}{|1-gF(\omega)|^2}, \tag{5.1}$$

where

$$F(\omega) = -\lim_{\eta\to 0} \int \frac{D(\omega')}{\omega-\omega'+i\eta}\, d\omega'. \tag{5.2}$$

Here, $D(\omega)$ is the joint density of states, which in two dimensions is constant above the band gap. In the limit $g = 0$, the dielectric function in Eq. (5.1) reduces to the usual result for interband transitions. However, the electron-hole interaction enhances the matrix elements near threshold.

To complete the description of the charge-transfer absorption band, one must include polaron effects. Early evidence that charge carriers form polarons comes from the measurements of Chen *et al.* (1989, 1991) of the dielectric constant of La_2CuO_{4+y}. They showed that when $y = 0$, the static dielectric constant is $\varepsilon_s = 31 \pm 2$ for electric field parallel to the CuO_2 layer and 27 ± 2 for electric field perpendicular to the layer. This is discussed in more detail below. The optical frequency value $\varepsilon_\infty = 5$ is much smaller because most of the polarization comes from optical phonons. Chen *et al.* (1991) pointed out that, since the Fröhlich electron-optical-phonon coupling constant is given by

$$\alpha_p = \frac{e^2}{4\hbar\omega_0}\left(\frac{1}{\varepsilon_\infty}-\frac{1}{\varepsilon_s}\right)\left(\frac{2m^*\omega_0}{\hbar}\right)^{1/2}, \tag{5.3}$$

the large difference between ε_s and ε_∞ implies that α_p is large and that the charge carriers form polarons. Here, m^* is the band effective mass in the absence of electron-phonon coupling, and ω_0 is the frequency of the LO phonon resulting in the large difference between ε_s and ε_∞. Falck *et al.* (1992) introduced into the dielectric function [Eqs. (5.1) and (5.2)] the temperature dependence of the band gap

$$E_g(T) = E_0 - 2\hbar\omega_0\alpha_p[n(\hbar\omega_0/kT)+1] \tag{5.4}$$

and that of the lifetime

$$\eta(T) = 2^{2/3}\omega_0(\hbar\omega_0/E)^{1/2}\alpha_p[2n(\hbar\omega_0/kT)+1], \tag{5.5}$$

predicted by polaron theory. Here, n is the Bose-Einstein occupation number. The average phonon en-

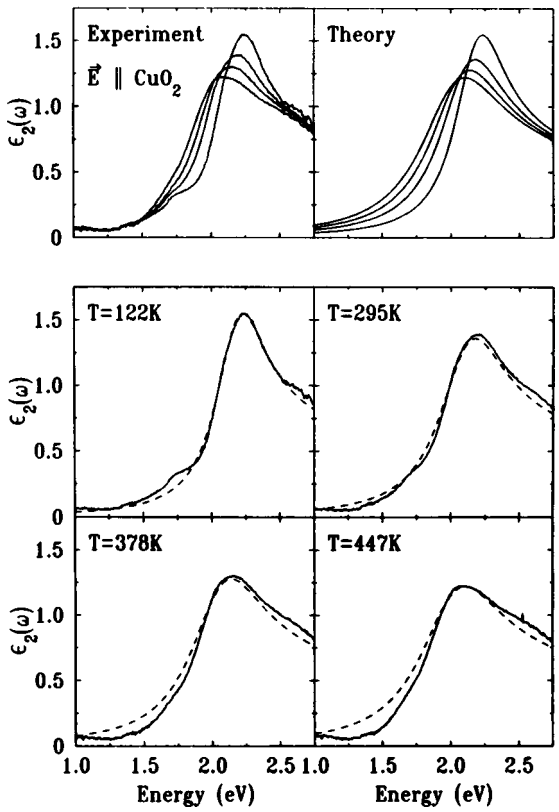

FIG. 17. The in-plane $\varepsilon_2(\omega)$ for four different temperatures together with the best fit to the data using the model discussed in the text. All four temperatures are shown in the upper two panels; theory and experiment are compared for individual temperatures in the lower four panels. From Falck *et al.* (1992).

ergy, $\hbar\omega_0 = 0.043 \pm 0.004$ eV, is determined by the shift of the peak in reflectivity with temperature, which reflects that of the gap [Eq. (5.4)], Falck *et al.* (1992) fitted the ε_2 spectrum at low T. However, the spectrum was then predicted without further adjustment up to 447 K, as illustrated in Fig. 17. The low-T fit gives $\alpha_p = 5.7$, which puts the large polarons in La_2CuO_4 in the intermediate coupling regime.

Confirmation of this picture comes from Fig. 18, which shows data of Uchida *et al.* (1991) for the optical conductivity spectra, derived from the reflectivity, of $La_{2-x}Sr_xCuO_4$. From a fit to the Drude-like behavior at low photon energy, these authors found that the holes induced by Sr have effective mass of ~ 2 times the free-electron mass, m_e. The polaron mass is given by $m_p = (1+\alpha_p/6)m^*$ (Feynman, 1955; Appel, 1968). Substitution of our value $\alpha_p = 5.7$ gives $m^* = 1$. Photoemission results on $Sr_2CuO_2Cl_2$ agree with this, as discussed in Sec. VI.

C. Impurity ionization spectrum

The charge-transfer spectrum thus provides strong evidence that free electrons and holes form large polarons. However, infrared measurements on lightly

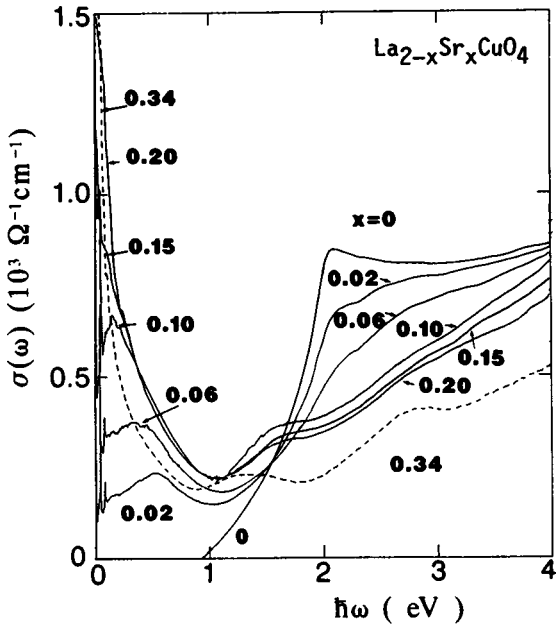

FIG. 18. Optical conductivity $\sigma(\omega)$ for various x obtained from the reflectivity measured with the electric field parallel to the CuO_2 layers. From Uchida *et al.* (1991).

doped La_2CuO_4 imply that bound holes form polarons that are small (Falck *et al.*, 1993), Figure 19 shows the reflectivity and ε_2 spectra for La_2CuO_{4+y} with $y = 0.014$. The reflectivity for the undoped compound is shown for comparison. This spectrum is for lower energies than for those in Fig. 16. The in-plane reflectivity spectrum for the doped crystal reveals two bands. The one at ~ 0.5 eV, found in many high-T_c materials and their lightly doped parent materials (Thomas, 1991), is nearly temperature independent. However, a second band, at 0.13 eV, is very strongly temperature-dependent. It is this band that we associate with small polarons. Figure 20 shows results of Thomas *et al.* (1992) that show the two bands quite clearly. Note that the broad band at ~ 0.6 eV in La_2CuO_{4+y} has the same position and width as the intrinsic broad spectrum in the carrier-free material (Fig. 12). Falck *et al.* (1993) show that the decrease with T of the oscillator strength in the 0.13 eV band is equal to the increase in the strength of the Drude peak, as determined from the dc conductivity measured by Preyer *et al.* (1989). These transport results are reviewed in Sec. VI.

Indeed, as illustrated in Fig. 21, Falck *et al.* (1993) quantitatively predict the T dependence of the reflectivity peak corresponding to the 0.13 eV peak in ε_2 with a model in which the holes form small polarons when bound to impurities. The shape of the peak in ε_2 is also consistent with this model. As the temperature is raised, the polarons are thermally ionized with the small binding energy of ~ 30 meV. As usual, the strong electron-phonon coupling via the Frank-Condon principle makes the optical ionization energy much larger than the thermal energy. The most sensitive parameter in the model is the thermal ionization energy, which was determined independently from the temperature dependence of the

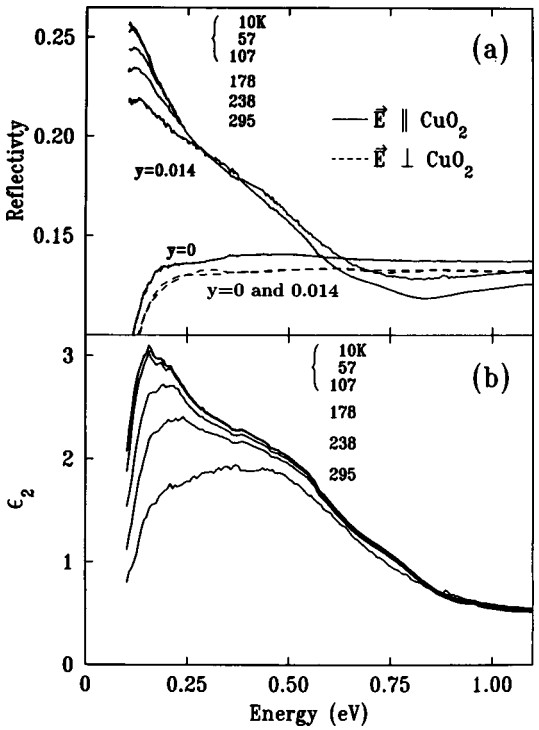

FIG. 19. Spectra of La_2CuO_{4+y}: (a) Temperature dependence of the reflectivity spectra of La_2CuO_{4+y} with $y = 0$ and 0.014. The in-plane spectra for the doped sample are indistinguishable below $\sim$ 100 K. Above 0.3 eV they are displayed only for 10 and 295 K, with the latter having the higher reflectivity. (b) In-plane $\varepsilon_2(\omega,T)$ for the oxygen-doped sample. From Falck *et al.* (1993).

Hall coefficient by Preyer, Birgeneau, Chen *et al.* (1989). The number of phonons coupled to the hole is $\sim$ 5 for the small polaron, just as it is for the large one ($\alpha_p \sim 5$). However, the large difference between the thermal ionization energy (0.035 eV from Preyer, Birgeneau, Chen *et al.*, 1989) and the optical ionization energy (0.13 eV) provides strong evidence that the polarons are small when bound. This is confirmed by measurement of localized phonon modes associated with the bound holes (Calvani *et al.*, 1994; Capizzi *et al.*, 1994), Mihailovic *et al.*, (1990, 1991) have also found evidence for polaron formation.

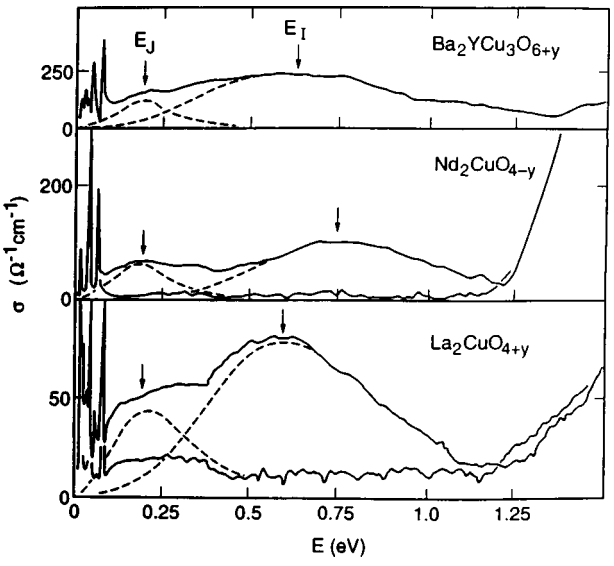

FIG. 20. Optical conductivity in lightly oxygen-doped $YBa_2Cu_3O_{6+y}$, Nd_2CuO_{4-y}, and La_2CuO_{4+y}. From Thomas *et al.* (1992).

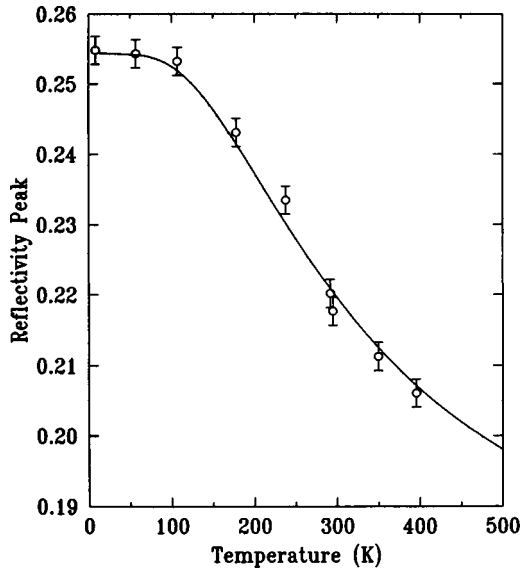

FIG. 21. Temperature dependence of the in-plane reflectivity at 0.11 eV. The solid line represents a fit to the data using a small-polaron model. From Falck *et al.* (1993).

Thomas and co-workers (Thomas, 1991; Thomas *et al.*, 1992) found that the 0.13 eV band persists to much higher temperature than was found by Falck *et al.* (1993). On the other hand, Kim *et al.* (1991) found that the same band when photoinduced disappears even more rapidly with increasing temperature. The photoinduced spectra of Kim *et al.* are shown in Fig. 22 and the temperature dependence is shown in Fig. 23. This shows that the optical energy is only weakly dependent on the thermal energy, consistent with the idea that the optical energy is dominated by the phonon contribution to the binding energy of the small polaron.

Optical measurements have thus provided a fairly complete characterization of the $q = 0$ electronic excitations in the photon energy range 0.1–3 eV for the pure and lightly doped CuO_2 layers. The sharp peak near 0.4 eV in the undoped materials results from the two-magnon quasibound state, made allowed by coupling to optical phonons. The broader bands extending up to $\sim$ 1 eV probably result from crystal-field excitons coupled to magnons.

VI. ELECTRONIC TRANSPORT IN UNDOPED AND LIGHTLY DOPED CuO_2 LAYERS

In this section we review what is known about the insulator-to-metal transition induced by the addition of charge carriers to the CuO_2 layers. We first discuss (Sec. VI.A) photoemission experiments that measure the dis-

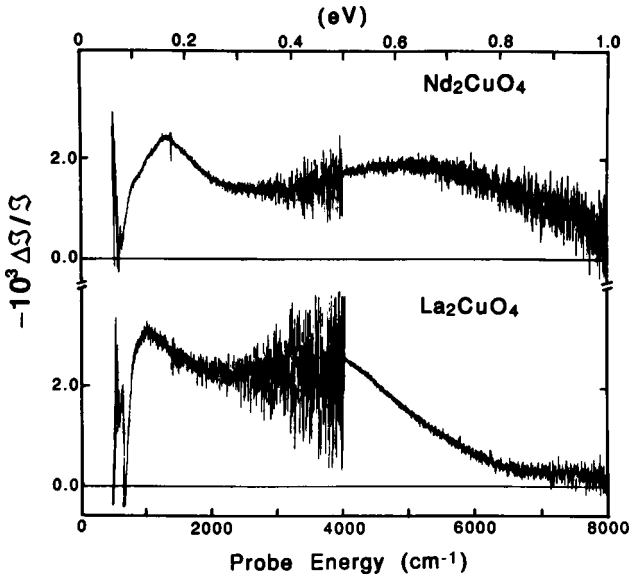

FIG. 22. Photoinduced optical absorption at $T = 4.2$ K. The quantity measured is the relative change in transmission upon excitation with above-band-gap (2.7 eV) light. From Kim *et al.* (1991).

persion relation for the highest-energy filled band in $Sr_2CuO_2Cl_2$. We then turn (Sec. VI.B) to the measurements of conductivity and the Hall effect in very lightly doped La_2CuO_4, which show that this material behaves like a conventional doped semiconductor, although the charge carriers are polarons, as demonstrated in the previous section. We review, in Sec. VI.C, measurements of the dielectric constant which illustrate that the insulator-to-metal transition occurs very close to the boundary of the 3D antiferromagnetic phase. Finally, in Sec. VI.D we discuss the peculiar properties of the metal at very low carrier concentration.

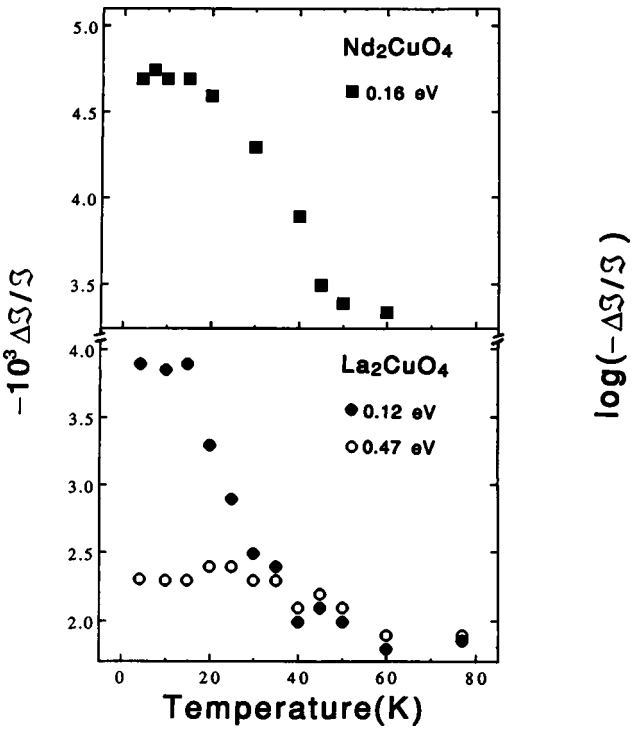

FIG. 23. Temperature dependence of the photoinduced absorption. From Kim *et al.* (1991).

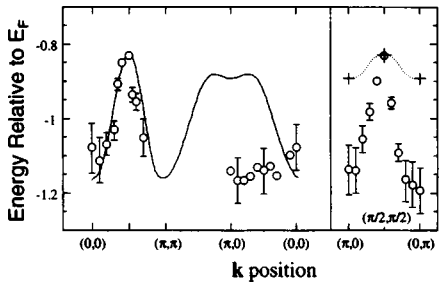

FIG. 24. Comparison of the experimentally determined E vs $\mathbf{k}$ relation (circles) with a calculation for the t-J model (Wells *et al.*, 1995). The right panel shows the direction along the antiferromagnetic zone edge for $(0,\pi)$ to $(\pi,0)$. For the latter only the points marked by a + are calculated and the dotted curve is the interpolation of Wells *et al.* (See Wells *et al.*, 1995, for details.)

A. Angle-resolved photoemission for $Sr_2CuO_2Cl_2$

Experiments over the past several years have shown the power of angular-resolved photoemission spectroscopy (ARPES) in determining the dispersion relation for positively charged quasiparticles in the CuO_2 layer. In this experiment the energy and momentum of the photoemitted electron are measured; these give the energy and momentum of the hole left behind. Wells *et al.* (1995) applied this technique to $Sr_2CuO_2Cl_2$. Since crystals of this material are free of charge carriers as grown and since they are easily cleaved, which facilitates ARPES, this is an ideal material for studies of the dispersion relation for holes in the undoped CuO_2 layer.

Figure 24 compares the results of Wells *et al.* (1995) with a calculation based on the t-J model, which describes the motion of the hole by including nearest neighbor hopping with matrix element t and coupling between nearest neighbor spins with antiferromagnetic exchange J. The highest energy filled electron band is well described by the t-J model in the direction between the (0,0) point and the (π,π) point in k space, although not near $(\pi,0)$. The t-J model predicts a bandwidth of $2.2J$—Wells *et al.* found the same value within the errors using $J = 125$ meV (Tokura *et al.*, 1990). This is in contrast to the prediction of one-electron calculations, which find a bandwidth nearly ten times larger. In addition there is a strong variation in spectral weight as a function of $\mathbf{k}$, reflecting the antiferromagnetic order. Thus the strong correlations, evinced by the insulating antiferromagnetic state itself, are also evident in the dispersion relation of the holes.

Most recently, Kim *et al.* (1998) have succeeded in carrying out ARPES measurements in $Sr_2CuO_2Cl_2$ at 150 K, well below the Néel temperature. These data reveal detailed momentum-dependent lineshape changes as a function of wavevector. Specifically, while a sharp quasiparticle-like peak is observed near $(\pi/2,\pi/2)$,

broad peaks are observed near $(\pi,0)$. Following previous workers (Nazarenko *et al.*, 1995; Belinicher *et al.*, 1996; Kyung and Ferrell, 1996; Xiang and Wheatley, 1996; Eder *et al.*, 1997; Laughlin, 1997; Lee and Shih, 1997; Leung *et al.*, 1998) Kim *et al.* show that by generalizing the t-J model to include second- and third-neighbor hopping terms t' and t'', both the overall dispersion and the line shapes may be properly accounted for. Kim *et al.* also compare the $Sr_2CuO_2Cl_2$ data with ARPES results in underdoped and overdoped $Bi_2Sr_2CaCu_2O_{8+\delta}$. In brief, upon hole doping from the insulator to the overdoped superconductor, the quasiparticle peak at $(\pi,0)$ changes in three ways: it moves toward the Fermi energy; it becomes sharper; and it increases in intensity. In contrast, doping has relatively little effect on the peak near $(\pi/2,\pi/2)$. This general trend is qualitatively explained by the above-mentioned t-t'-t''-J model calculations.

For the present discussion we focus on a different feature of the data. The maximum of the band in Fig. 24 is at $(\pi/2,\pi/2)$. Presumably, holes added by doping in other materials containing CuO_2 layers reside near this point. Although the bandwidth is relatively small, the maximum is narrow in k space, resulting in an effective mass of 1.5 ± 0.75. Note that because ARPES takes place on a very short time scale, this mass does not include any polaron contribution. Thus while the electron correlations are evident in the band structure, reducing the overall band width to $2.2J$, they leave the mass of holes near the band maximum relatively light. At equilibrium, however, these holes are dressed by phonons, increasing the mass to ~ 2, as discussed in Sec. V.

B. Conductivity and hall effect in lightly doped La_2CuO_4

When La_2CuO_4 is doped with oxygen or Sr at levels below $\sim 1\%$ of the Cu atom density, it behaves like a conventional doped semiconductor. Figure 25, from Preyer, Birgeneau, Chen, *et al.* (1989) shows that the conductivity of La_2CuO_{4+y} is approximately thermally activated at high temperature; it follows the 3D variable-range hopping form $\sigma \sim \exp[-(T_0/T)^{1/4}]$ at low T. This is typical of the behavior of doped semiconductors (for an overview see Fritzsche, 1978). In such systems the acceptors give rise to an impurity band close in energy to the valence band, and at high temperature the conductivity is limited by the number of holes in the valence band. Because some of the acceptors are compensated by donors or defects, the Fermi energy lies in the impurity band and the ionization energy of the acceptors is approximately equal to the activation energy of the conductivity (Blakemore, 1969). Furthermore, the empty acceptor sites allow holes to hop from neutral to ionized acceptors giving rise to phonon-assisted tunneling, or hopping, at low T.

As the density of acceptors is increased, the interaction between acceptors broadens the impurity band causing the minimum ionization energy to decrease. Therefore, the activation energy of the conductivity decreases, going to zero when the impurity band merges

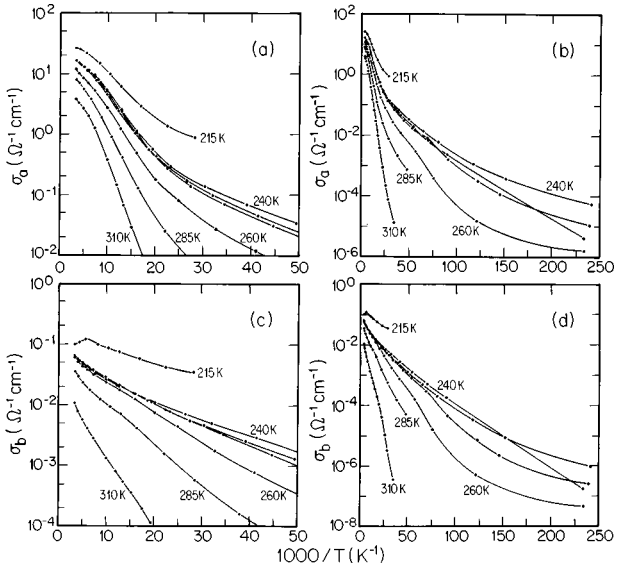

FIG. 25. Conductivity for directions parallel (σ_a) and perpendicular (σ_b) to the CuO_2 layer in La_2CuO_{4+y}. The curves are labeled by T_N, which decreases with increasing y. (a) and (c) show the higher temperatures ($T > 20$ K) and (b) and (d) the lower temperatures. Three different preparation procedures give the same T_N but different conductivity at low T. From Preyer, Birgeneau, Chen, *et al.* (1989).

with the valence band (Fritzsche, 1955; Fritzsche and Cuevas, 1960). Simultaneously, as the density of acceptors increases the hopping conductivity increases exponentially. This happens because the hopping rate is proportional to the overlap of wave functions on the initial and final sites, which varies as $\exp[-(R/2a_0)]$ where R is the distance between impurities and a_0 is the Bohr radius.

The Hall effect can be used to measure directly the binding energy of the hole to the acceptor. Chen *et al.* (1995) measured the Hall coefficient for single crystals of $La_2CuO_{4+0.001}$ and $La_{1.998}Sr_{0.002}CuO_4$, each containing 0.002 holes per Cu atom. The maximum in the Hall coefficient seen in Fig. 26 results from the competition between the higher-mobility band conduction with activated carrier density at high T to the lower-mobility hopping mechanism with weakly temperature dependent carrier density at low T (Fritzsche, 1955). The activation energy of the Hall density is the thermal ionization energy of the acceptor. In the inset of Fig. 26 this activation energy is plotted as a function of Néel temperature. For very lightly doped La_2CuO_{4+y}, for which the Néel temperature is high, the binding energy of the hole to the oxygen acceptor approaches $E_b = 35$ meV. The binding energy of the Sr acceptor is somewhat smaller, 19 ± 2 meV for the crystal containing 0.002 Sr per Cu. The crossover from hopping to band conduction occurs at a temperature considerably lower than E_b/k because the band mobility is much higher than the hopping mobility.

Chen *et al.* (1995) have quantitatively explained the magnitude and temperature dependence of the Hall mobility in the temperature regime in which band conductivity dominates over hopping conductivity. The mobil-

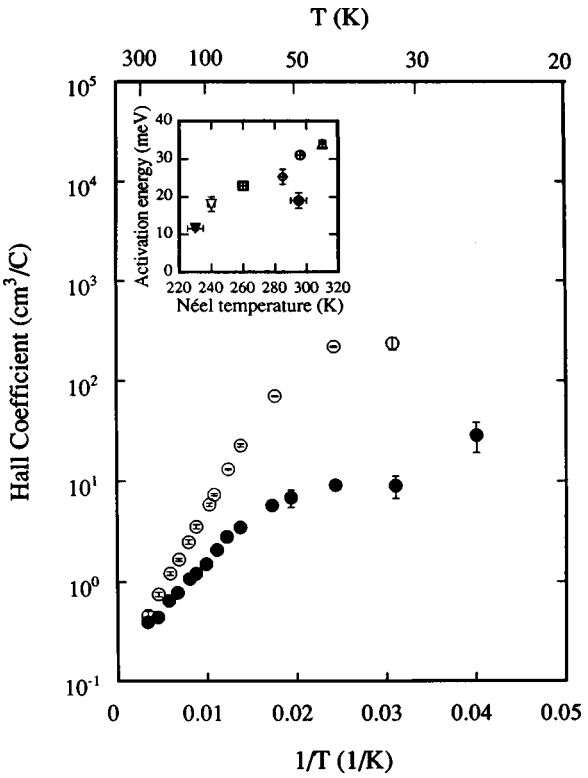

FIG. 26. Hall coefficient plotted on a semilog plot vs $1/T$ of La_2CuO_{4+y} (open circles) and $La_{2-x}CuO_4$ (closed circles) each containing 2×10^{-3} holes per Cu ion. The activation energies extracted from the straight lines at high T are plotted vs T_N in the inset, along with those for La_2CuO_{4+y} with other values of y, whose conductivities are shown in Fig. 25. From Chen *et al.* (1995).

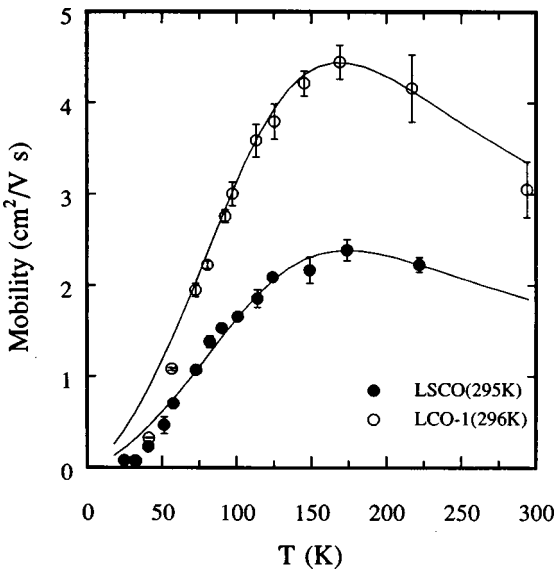

FIG. 27. In-plane mobilities of La_2CuO_{4+y} (open circles) and $La_{2-x}CuO_4$ (closed circles) each containing 2×10^{-3} holes per Cu ion. The data are determined from measurements of the conductivity and Hall coefficient, like those in Figs. 25 and 26. The solid curves are the results of fits to the model discussed in the text. From Chen *et al.* (1995).

ity is obtained directly from the relationship

$$\sigma = pe\mu = \frac{\mu}{R_H}, \tag{6.1}$$

where σ is the conductivity, p is the hole density, μ is the Hall mobility, and R_H is the Hall coefficient.

Equation (5.5) shows that large polarons are strongly scattered at high temperatures by the same optical phonons that lead to the polaron formation. Using Eq. (5.5), the mobility limited by optical phonon scattering is given approximately by

$$\mu_{op} = \frac{e}{2m^*\alpha_p} \exp\left[\frac{\hbar\omega_0}{kT}\right] \tag{6.2}$$

for $kT < \hbar\omega_0$. As the temperature increases, the number of phonons increases exponentially with $1/T$, and the mobility decreases accordingly.

At lower temperatures the most important scattering mechanism for doped semiconductors is scattering by charged impurities, usually described by the Brooks-Herring (Brooks, 1955) model of Rutherford scattering from the screened Coulomb potential. When this mechanism dominates for a semiconductor with isotropic effective mass, the mobility is given by

$$\mu_I = A T^{3/2}. \tag{6.3}$$

The mobility increases with T because the rate of Rutherford scattering of an electron by an ionized impurity decreases with increasing velocity of the electron, and the latter increases with T.

If scattering from polar optical phonons and from ionized impurities is dominant the mobility is thus predicted to be

$$\frac{1}{\mu} = \frac{1}{\mu_I} + \frac{1}{\mu_{op}} = A\left(\frac{1}{T}\right)^{3/2} + B \exp\left(-\frac{\hbar\omega_0}{kT}\right), \tag{6.4}$$

where the coefficient B is predicted by Eq. (6.2). At low temperatures, where the scattering by ionized impurities dominates, the mobility increases with temperature, whereas at high temperatures, where the scattering is dominated by optical phonons, the mobility decreases with temperature. Falck *et al.* (1992) found that the choice $\hbar\omega_0 = 0.043 \pm 0.004$ eV provided the best fit for the T dependence of the charge transfer gap, as discussed above. With $\hbar\omega_0$ fixed at 0.043 eV, the maximum value of the mobility $\mu_{\max}$ and the corresponding temperature $T_{\max}$ uniquely determine A and B in Eq. (6.4). Using the values of A and B determined this way, the fit to the data is very good, as can be seen in Fig. 27. The theoretical prediction (solid curve) is consistent with the experimental results above $\sim$ 60 K. At lower temperatures the experimental mobilities are smaller than the theoretical predictions. However, this is the temperature range in which hopping conduction dominates. Because the effective mobility of hopping conduction is much smaller than that of the band conduction, the Hall mobility, which is a weighted sum of the two, is then expected to be smaller than predicted.

Not only is the overall temperature dependence predicted properly by Eq. (6.4), but also the magnitude of

the optical phonon contribution to the scattering is predicted. Using the values $\hbar\omega_0 = 0.043 \pm 4$ eV and $\alpha_p = 5.7$, determined by Falck *et al.* (1992) from optical measurements, and the value $m_p = 2m_e$ determined from optical and transport measurements (Chen *et al.*, 1989; Chen *et al.*, 1991; Uchida *et al.*, 1991; Falck *et al.*, 1992), the parameter B that appears in Eq. (6.4) is simply related to the prefactor in Eq. (6.2) to be 0.85 V s/cm^2. The values of B determined from the measured mobilities as discussed above are 1.4 and 2.5 V s/cm^2 for oxygen and Sr doping, respectively. These are in quite good agreement with the prediction, considering that the phonon frequency, which appears in the exponent and therefore influences the determination of B quite strongly, is an average over several optical phonons, and is only determined to $\sim 10\%$ by Falck *et al.*

The ionized-impurity scattering coefficient A is found to be about 10 times smaller than that predicted by theory. This kind of discrepancy is common even for conventional semiconductors (Chattopadhyay and Queisser, 1981). It is thought that the Born approximation may be inadequate or that other simplifying assumptions in the Brooks-Herring treatment may not be valid. In addition, for La_2CuO_4 the reduced dimensionality may make the Brooks-Herring treatment insufficient.

The quantitative agreement between the optical phonon scattering rate and the prediction of polaron theory provides strong confirmation of the conclusion, drawn from the temperature dependence of the charge-transfer absorption (Sec. V.B), that the free holes form large polarons. Furthermore, from the temperature dependence of the impurity-induced infrared absorption (Sec. V.C), it is clear that bound holes form small polarons. This raises the question of whether polarons survive in the metallic phase or whether the electron-hole interaction is screened by the large carrier concentration. This is still an open question, whose answer may be helpful in elucidating the mechanism of high-temperature superconductivity.

C. Dielectric constant near the insulator-to-metal transition

The acceptor state created by adding excess oxygen to La_2CuO_4 has been characterized in some detail using dielectric-constant measurements (Chen *et al.*, 1989; Chen *et al.*, 1991). The real part of the dielectric function ε_1 decreases as a power law with frequency at low frequency because of the hopping of holes between acceptors. This and the corresponding behavior of the ac conductivity, also reported by Chen *et al.* (1989, 1991) is typical of doped, compensated semiconductors.

At high frequency, ε_1 saturates at a value ε_s that depends on field direction and oxygen content. The dielectric constant is plotted in Fig. 28 as a function of hole concentration, which is determined from the room-temperature value of the Hall coefficient. In the limit of zero hole concentration, when the shallow acceptors are

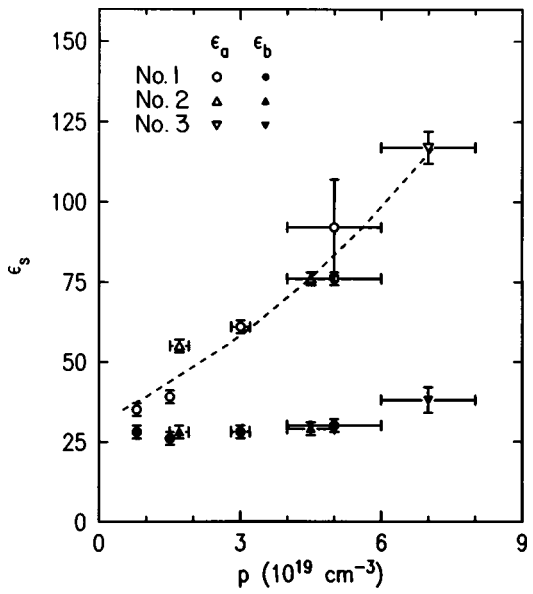

FIG. 28. The dielectric constant ε_s measured at a high enough frequency to eliminate the hopping contribution, but low enough to include all others. The hole concentration is determined from the room-temperature value of the Hall coefficient. The curve is a guide to the eye, illustrating the growth of ε_s for the in-plane (ε_a) but not the out-of-plane (ε_b) direction. From Chen *et al.* (1991).

eliminated, the dielectric constant of the host material ε_h is fairly isotropic: the values are 31 ± 2 and 27 ± 2 for the a and c directions, respectively. As demonstrated by the infrared studies of Collins *et al.* (1989), the dielectric constant is dominated by the contribution of phonons with energies in the range 30–60 meV. A similarly large value of ε_s is found in $YBa_2Cu_3O_6$ (Samara *et al.*, 1990). While moderately large, the values of the dielectric constant are typical of many oxides. For example, for BaO $\varepsilon_h = 34$, for CuO $\varepsilon_h = 18$, and for PbO $\varepsilon_h = 26$.

As the hole concentration increases, the dielectric constant increases dramatically but only for the in-plane polarization, as seen in Fig. 28. For low density one has

$$\varepsilon_s - \varepsilon_h = 4\pi N_A \alpha_{\rm pol}, \tag{6.5}$$

where N_A is the acceptor density, $\alpha_{\rm pol}$ is the polarizability. From a linear fit to the increase of ε_s with density (Fig. 28) Chen *et al.* (1991) find that $\alpha_{\rm pol} = (4 \pm 1) \times 10^{-20}$ cm^3. We next review their argument that this value of the polarizability and the measured binding energy of the hole to the acceptor are consistent with a simple hydrogenic model if one uses the host dielectric constant $\varepsilon_h = 30$ to screen the Coulomb interaction and if one sets the charge-carrier mass equal to the polaron mass.

Recall that the Bohr model gives for the impurity binding energy

$$E_b = 13.6 \text{ eV} \left(\frac{m_p}{m_e}\right) \varepsilon_h^{-2}, \tag{6.6}$$

where m_p is the polaron mass, and gives for the radius,

$$a_0 = 0.529\ \text{Å}\,\frac{m_e}{m_p}\,\varepsilon_h . \tag{6.7}$$

As discussed in Sec. V, the polaron mass is given by $m_p = (1 + \alpha_p/6)m^*$, so with $\alpha_p \sim 6$ and $m^* \sim m_e$, from the photoemission results discussed above, this yields $m_p = 2m_e$. Substituting this value of m_p and $\varepsilon_h = 30$ into Eqs. (6.6) and (6.7) gives $E_b = 30$ meV and $a_0 = 8$ Å. For a hydrogenic impurity in a material with dielectric constant ε_s one has $\alpha_{\text{pol}} = \frac{9}{4}\varepsilon_h a_0^3$, and thence Chen *et al.* (1991) find from their value of α_{pol} that $a_0 = 8 \pm 2$ Å, also consistent with Eq. (6.7).

This value of the in-plane radius is consistent with the rapid growth of the in-plane dielectric constant. When the density is raised to $7 \times 10^{19}\ \text{cm}^{-3}$, which is 0.7% holes per Cu atom, the in-plane value of ε_s is more than 100. To achieve such high values of ε_s in *P*-doped Si, for example, one must reach densities within $\sim 10\%$ of the critical concentration for the insulator-to-metal transition (Paalanen *et al.*, 1983). The critical concentration can be calculated from the Mott criterion: $n_c^{1/3} a_0 = 0.23$. For a radius of 8 Å, the critical density is $\sim 2 \times 10^{19}\ \text{cm}^{-3}$. Thus this model predicts that with a density of $7 \times 10^{19}\ \text{cm}^{-3}$, La_2CuO_4 should be metallic. However, because it is two dimensional, the insulator-to-metal transition does not occur at this point.

Close to a 3D transition, the dielectric constant, which scales like the square of the localization length, diverges because the localization length diverges. However, the growth of ε_s in Fig. 28 is clearly two-dimensional rather than three-dimensional, and in 2D there is no transition because all states are localized at zero temperature (for a review see Lee and Ramakrishnan, 1985). This explains why ε_s, although growing quite large, does not appear to diverge. We return to this issue of the dimensionality of the insulator-to-metal transition in our discussion of heavily-doped crystals.

Objections can be raised to the use of the simple hydrogenic model for the hole bound to the acceptor. As seen from the anisotropy of the growth in the dielectric constant, the hole is apparently confined to a single layer. Because of this, the potential is not truly Coulombic. Chaillout *et al.* (1989, 1990) concluded from neutron measurements on heavily oxygenated La_2CuO_{4+y} that the oxygen acceptor lies near the midpoint between two adjacent CuO_2 layers, but slightly closer to one layer than to the other. The potential seen by a hole confined to a single layer is approximately

$$V(r) = \frac{e^2}{\varepsilon_h \sqrt{r^2 + d^2}},$$

where r is the distance within the CuO_2 layer and d is the perpendicular distance from the acceptor to the layer. This potential gives a more weakly bound state than the corresponding Coulomb potential. However, a two-dimensional model, like the three-dimensional one, gives a consistent description with a binding energy of 35 meV and a radius of 8 Å (Serre *et al.*, 1989; Gold, 1991).

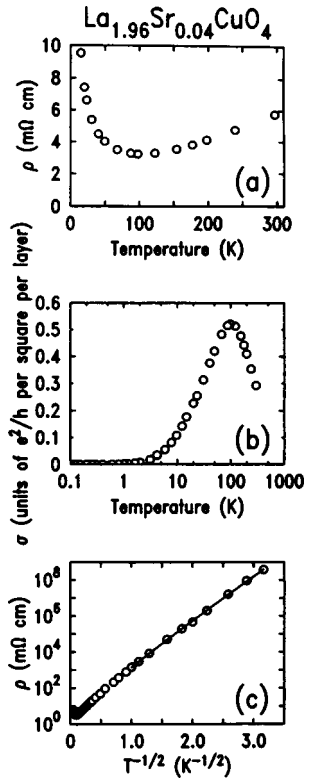

FIG. 29. In-plane resistivity of single-crystal $La_{1.96}Sr_{0.04}CuO_4$: (a) Resistivity. (b) Two-dimensional conductance per square per CuO_2 layer, plotted vs $\log_{10} T$. (c) Low-temperature in-plane resistivity, plotted such that the functional dependence $\rho \sim \exp(T_{CG}/T)^{1/2}$ is highlighted. The solid line is a fit to this form, which results from hopping in a Coulomb gap. From Keimer, Belk, *et al.* (1992).

Rabe and Bhatt (1991) argued that the Coulomb potential is screened only by the optical dielectric constant ε_{op} instead of ε_h. The use of ε_h implies that most of the screening comes from phonons because the dielectric constant at frequencies above those of the phonons falls to $\varepsilon_{\text{op}} \sim 5$. Rabe and Bhatt calculated the binding energy of the hole to the Sr impurity using the smaller dielectric constant and found a value near 0.5 eV. It is clear from Fig. 26 that such a large value of the binding energy cannot be reconciled with experimental observations. Furthermore, because of the large binding energy, Rabe and Bhatt find that the insulator-to-metal transition occurs at $\sim 20\%$ holes instead of the observed 2%.

D. Conductivity and magnetoresistance in the spin-glass regime

As we have seen, the dielectric constant of La_2CuO_{4+y} becomes very large in the vicinity of the boundary of the antiferromagnet, near 2% holes per Cu, suggesting that the crossover from insulator to 2D metal occurs there. Controlling the Sr concentration in $La_{2-x}Sr_xCuO_4$ is very difficult, so the evolution with x at low x of the dielectric constant and conductivity have not been measured in single crystals of the latter system.

However, for $x \sim 2-4\%$, it appears that many features of the peculiar metal, which is the normal state of the high-T_c superconductor, are already established.

Figure 29 shows the in-plane resistivity plotted in various ways for a crystal of $La_{1.96}Sr_{0.04}CuO_4$. As discussed below, this same crystal has recently been shown to have all the features of a conventional spin glass (Chou *et al.*, 1995). The top panel shows that above 100 K the resistivity increases linearly with T. As pointed out by Preyer *et al.* 1991), the slope of ρ vs T with the density of carriers given by $x = 0.04$ gives a scattering rate $\sim h/kT$, the same as for the normal state of the highest-T_c superconductors. This is a very important result: as soon as the density is high enough to destroy the antiferromagnetic long-range order, the system displays this unusual scattering.

As shown in Fig. 29(b), the conductance below $\sim$ 100 K decreases with decreasing T. The decrease is approximately logarithmic for about a decade of temperature, with a coefficient that is of order e^2/h (the quantum of conductance) per square per CuO_2 layer. This is typical of two-dimensional metals (Lee and Ramakrishnan, 1985). In such systems, disorder causes all states to be localized at $T = 0$. At very high T, where the inelastic scattering length $L_{\rm in}$ is less than the elastic scattering length l, the T dependence of the conductance is determined by that of $L_{\rm in}$. As T decreases $L_{\rm in}$ grows and when it exceeds l, logarithmic corrections to the conductance become apparent. At still lower T, when $L_{\rm in}$ becomes greater than the localization length λ, the system becomes strongly localized. This is seen clearly in Fig. 29(c). The plot shows that the resistivity follows $\rho \sim \exp(T/T_0)^{1/2}$, characteristic of variable-range hopping in a Coulomb gap (Shklovskii and Efros, 1984). The crossover temperature between ln T and exponential temperature dependence indicates that, for this sample, $\lambda \sim 10 \sim 100$ Å.

Figure 30 shows resistivity data of Takagi *et al.* for ceramic samples of $La_{2-x}Sr_xCuO_4$ (Takagi *et al.*, 1992). Note that the resistance is linear in temperature only for samples with x below $\sim$ 0.2.

Very recent results of Ando, Boebinger, and coworkers show that the logarithmic T dependence seen in Fig. 29 persists in the superconductors (Ando *et al.*, 1995; Ando *et al.*, 1996; Boebinger *et al.*, 1996). Using pulsed magnetic fields up to 60 T they are able to suppress the superconductivity and examine the normal-state resistivity. Figure 31 illustrates that both the in-plane resistivity ρ_{ab} and the out-of-plane resistivity ρ_c vary as log T below about 100 K, just as for the nonsuperconducting sample in Fig. 29. For doping levels beyond that for maximum T_c, the T dependence becomes characteristic of conventional metals. Thus this peculiar log T behavior, which is seen for hole concentrations as low as 2% per Cu atom, seems to be intrinsic to the unusual metal for less than optimal doping.

In all respects, the data of Fig. 29 are typical of a 2D metal. However, we will see that the underlying physics is quite different from that in conventional 2D systems. After we discuss the influence of charge carriers on the magnetism in the next section, we return to this crystal, which shows evidence that the magnetism influences the transport in important ways.

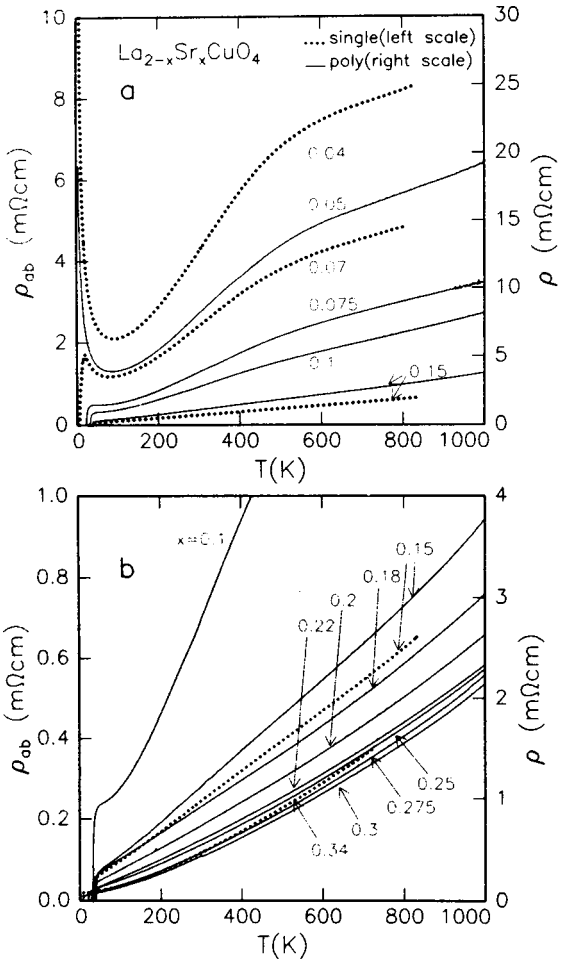

FIG. 30. The temperature dependence of the resistivity for $La_{2-x}Sr_xCuO_4$: (a) samples with x from 0.04 to 0.15 and (b) samples with x from 0.1 to 0.35. Dotted curves are the in-plane resistivity ρ_{ab} of single-crystal films with (001) orientation; solid lines are the resistivity ρ of polycrystalline samples. From Takagi *et al.* (1992).

VII. EVOLUTION OF THE MAGNETISM WITH DOPING

A. Destruction of the Néel state by electrons and holes

As seen in Fig. 1, the Néel temperature decreases rapidly from its maximum of 325 K when La_2CuO_4 is doped with Sr. Chen *et al.* (1991) used Hall measurements to determine T_N as a function of the density of shallow acceptors in La_2CuO_{4+y}; the results are shown in Fig. 32 (Keimer, Aharony, *et al.*, 1992). A straight-line extrapolation of the data gives T_N vanishing at $\sim$ 2% holes per Cu atom for oxygen doping, just as for Sr doping (Fig. 1).

The comparison between the effect of hole doping and that of electron doping in Fig. 32 is very dramatic. The reduction of T_N by Ce doping in $Pr_{2-x}Ce_xCuO_4$ and in $Nd_{2-x}Ce_xCuO_4$ (Matsuda *et al.*, 1992) is much more gradual than that of oxygen or Sr doping in

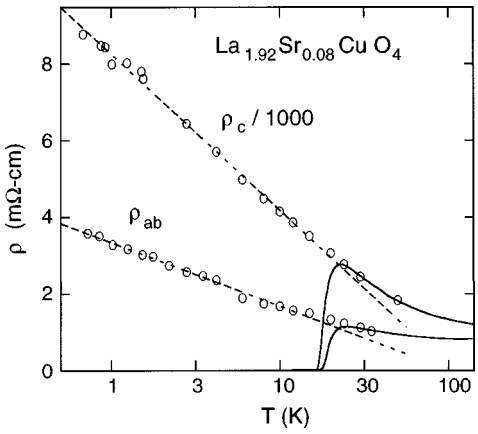

FIG. 31. In-plane (ρ_{ab}) and out-of-plane (ρ_c) resistivities of superconducting $La_{1.92}Sr_{0.08}CuO_4$. The solid curves are for zero magnetic field and the circles are measurements taken with a 60 T pulsed magnetic field, used to suppress the superconductivity. From Ando *et al.* (1995, 1996) and Boebinger *et al.* (1996).

$La_{2-x}Sr_xCuO_4$. Keimer, Aharony, *et al.* (1992) showed that Zn doping of La_2CuO_4 reduces T_N at the same rate as Ce doping of $Pr_{2-x}Ce_xCuO_4$. Since Zn substitutes for Cu but has one more valence electron, its addition increases the number of electrons in the CuO_2 layer as presumably does Ce doping in $Pr_{2-x}Ce_xCuO_4$. However, in the case of Zn doping the electron is tightly bound, whereas the nearly metallic conductivity resulting from Ce doping shows that the electrons in the latter case are more mobile (Hirochi *et al.*, 1989). Since Zn doping clearly results in dilution of the Cu spin system, the similarity of Ce doping suggests that electron doping always does so.

Matsuda *et al.* (1992) showed that the reduction of T_N in the electron-doped materials is the result of a reduction in the spin stiffness constant ρ_s. Indeed, their ratio of ρ_s in $Nd_{1.85}Ce_{0.15}CuO_4$ with $T_N = 160$ K to that in

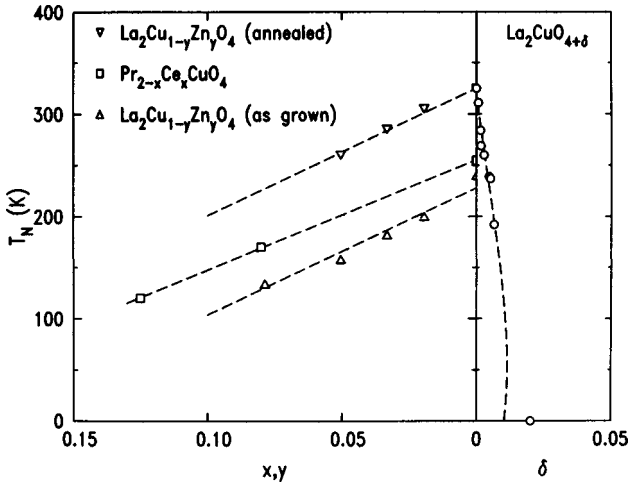

FIG. 32. Néel temperature as a function of electron and hole concentration. For the latter data from Chen *et al.* (1991), the hole concentration was determined using the Hall effect. From Keimer, Aharony, *et al.* (1992).

Nd_2CuO_4 is just that predicted by Harris and Kirkpatrick (Harris and Kirkpatrick, 1977) for dilution of the square lattice by $\sim 15\%$. It is quite clear, therefore, that the effect of electron doping is dilution of the 2D spin system.

By comparison with the electron-doped materials, the density of holes necessary to destroy the antiferromagnetic long-range order is surprisingly small. Instead of dilution, Aharony *et al.* (1988) proposed that excess holes, because they reside primarily on oxygen atoms, introduce frustration. The frustration occurs, in the model of Aharony *et al.*, because the exchange interaction between the hole on an oxygen and each of its two neighboring Cu holes, whether ferromagnetic or antiferromagnetic, is obviously the same, requiring that the Cu spins be parallel. However, the superexchange is antiferromagnetic, requiring opposite spins on Cu nearest neighbors. If the O-Cu exchange is large enough, the antiferromagnetic order will be disrupted, and because of the two dimensionality, following the arguments of Villain (1977, 1978), the disruption decays slowly with distance (see also Glazman and Ioselevich, 1989). Thus a small density of holes has catastrophic consequences for the long-range order. The classical arguments of Aharony *et al.* (1988) are substantiated in quantum Monte Carlo calculations (Morgenstern, 1990).

A simple generalization of the above model applicable to $La_{2-x}Sr_xCuO_4$ is to allow the hole to circulate either clockwise or counterclockwise in the oxygen plaquette directly above or directly below the Sr impurity. The hole motion couples to the transverse fluctuations of the Cu spins and produces a spiraling twisting of the antiferromagnetic order parameter, a state that is topologically similar to the singly charged skyrmion excitations of the 2D classical nonlinear sigma model. Gooding and Mailhot (Gooding, 1991; Gooding and Mailhot, 1993) proposed that a simple way of representing the effects of this circulating hole motion on the antiferromagnetic background is to integrate out the hole motion and replace it by a purely magnetic interaction. With (1,2,3,4) denoting the four spins in the plaquette bordering the Sr impurity, the interaction Hamiltonian of a single hole is given by

$$H_{\rm int} = -\frac{D}{S^4}[(\mathbf{S}_1\cdot\mathbf{S}_2\times\mathbf{S}_3)^2+(\mathbf{S}_2\cdot\mathbf{S}_3\times\mathbf{S}_4)^2 + (\mathbf{S}_3\cdot\mathbf{S}_4\times\mathbf{S}_1)^2+(\mathbf{S}_4\cdot\mathbf{S}_1\times\mathbf{S}_2)^2]. \quad (7.1)$$

One may show that, for classical spins, as long as $D/J > 2.2$, the ground state has the same topology as that of the circulating hole ground state. The spin distortions produced by these circulating holes are similar to the dipolar backflow spin distortions induced by mobile holes in the theories of Shraiman and Siggia (1988, 1989a, 1989b).

In the above models, for purely Heisenberg interactions the 2D long-range order is destroyed by a single hole even at $T = 0$. This occurs because of the long-range nature of the resultant spin distortion as first noted by Villain (1977, 1978). A transition to long-range order will occur only if the limiting 2D Heisenberg cor-

relation length at $T = 0$ is above a threshold value such that either the Ising anisotropy or the residual 3D interaction is able to drive the ordering [cf. Eq. (4.10)].

An alternative to the above is the so-called Zhang-Rice singlet model (Zhang and Rice, 1988). These authors mapped the three-band model into a single-band effective Hamiltonian. Cu-O hybridization then strongly binds a hole on each square of O atoms to the central Cu^{2+} to form a local spin singlet. This moves through the lattice in a way similar to a hole in the single-band effective Hamiltonian of the strongly interacting Hubbard model. If one includes only nearest-neighbor hopping then this model has particle-hole symmetry and this manifestly cannot describe the large difference between the electron- and hole-doped materials. This may be ameliorated by inclusion of more distant neighbor hopping terms which violate the electron-hole symmetry.

At low temperatures in the lightly doped regime, when the holes are known to become localized by disorder effects, one cannot describe the system by a Zhang-Rice singlet localized to a single Cu site. Specifically, this problem is isomorphic to the percolation problem, which does not at all describe the phase diagram or correlation lengths of the hole-doped materials. However, in the spirit of the Gooding model discussed above, the hole will delocalize around a single plaquette surrounding a Sr^{+2} impurity. This subsequently will form a spin distortion field similar in character to that generated by a localized oxygen hole (R. J. Gooding, private communication).

B. The spin glass regime

Aharony *et al.* (1988) have predicted that spin glass behavior would be observed just on the high-density side of the antiferromagnetic phase boundary at low T in Fig. 1. Evidence for slowing down of the spin fluctuations has been observed in neutron scattering (Keimer, Belk, *et al.*, 1992), muon spin relaxation (μSR) (Kumagai *et al.*, 1987; Budnick *et al.*, 1988; Harshman *et al.*, 1988; Mezei *et al.*, 1988; Uemura *et al.*, 1988), and nuclear quadrupole resonance (NQR) (Kitaoka *et al.*, 1988; Chou *et al.*, 1995). Recently, Chou *et al.* (1995) studied a piece of the very same crystal of $La_{1.96}Sr_{0.04}CuO_4$, whose conductance is shown in Fig. 29. They showed that this sample displays all of the behavior typical of canonical spin glasses: irreversibility and remnant magnetization below the glass transition and scaling behavior above and below it. Surprisingly, whereas the neutron measurements (Keimer, Belk *et al.*, 1992) show that there is one spin per Cu atom, the effective density of free spins contributing to the Curie susceptibility above the spin glass transition temperature is only 0.5% of the Cu atom density. Nonetheless, the spin glass transition temperature is in good agreement with that measured with μSR and NQR, which measure the freezing of all the Cu spins. This shows that the spin glass properties measured by Chou *et al.* (1995) reflect those of the entire Cu spin system. Calculations based on Eq. (6.1) with holes circulating around randomly situated Sr^{2+} impurities account for both the $T = 0$ correlation length and the 0.5% spin density. However, it remains to be understood why a model for localized holes should be so successful in this intermediate doping regime (Gooding *et al.*, 1997).

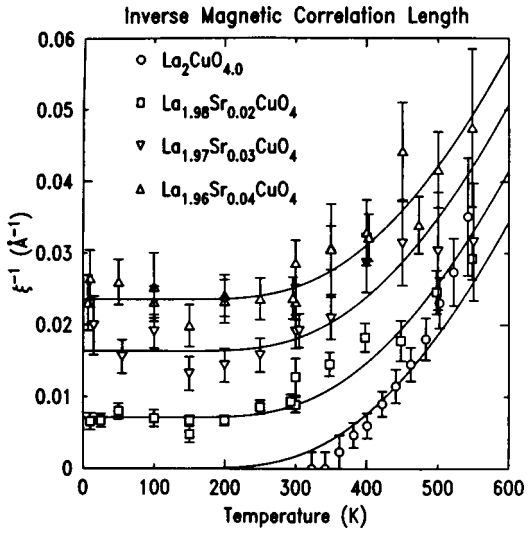

FIG. 33. Inverse magnetic correlation length of four crystals of $La_{2-x}Sr_xCuO_4$. The solid lines are calculated from $\kappa(x,T) = \kappa(x,0) + \kappa(0,T)$. From Keimer, Belk *et al.* (1992).

The simplest heuristic model for the evolution of the magnetism with doping near the antiferromagnetic phase boundary is based on the theory of Charkravarty, Halperin, and Nelson (CHN) (Chakravarty *et al.*, 1989). Their theory involves a mapping of the 2DSLHQA into the 2D quantum nonlinear sigma model. The latter has three basic regimes: (a) the renormalized classical regime where the correlation length follows $\xi \sim \exp(2\pi\rho_s/kT)$, achieving long-range order at $T = 0$, as discussed in Sec. IV.D; (b) the quantum critical regime with $\xi \sim hc/kT$, where c is the spin-wave velocity; (c) the quantum disordered regime where ξ remains finite as $T \to 0$. To describe the effects of doping within this model, one assumes that the effect of the holes is to renormalize ρ_s to zero near $x \approx 0.02$; that is, one assumes an effectively homogeneous model. As a function of x, the T dependence of ξ would then evolve from behavior (a) at low x to (b) at the critical value of x, to (c) at high x. Such a picture necessitates that the quenched disorder accompanying the doping is irrelevant so that the doped system is effectively translationally invariant. The assumed renomalization of ρ_s to zero could have different origins: frustration as in the model of Aharony *et al.* (1988) and of Gooding *et al.* (1997) or disorder caused by the motion of the holes, as in Shraiman and Siggia (1988, 1989a, 1989b).

In order to probe the evolution predicted by the 2D nonlinear sigma model, Keimer, Belk *et al.* (1992) carried out a study of the instantaneous spin correlations in $La_{2-x}Sr_xCuO_{4+y}$, varying both x and y to create samples with a variety of hole concentrations between 0 and 0.04 per Cu. Results for the inverse correlation length $\kappa = \xi^{-1}$ for some of these samples are shown in Fig. 33. All four samples are described by a very simple

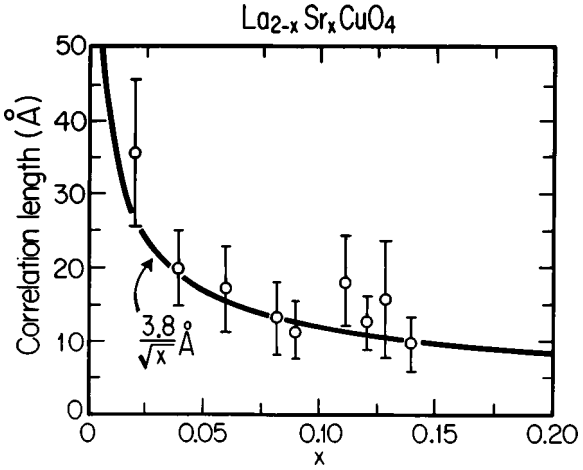

FIG. 34. Magnetic correlation length vs strontium concentration x. The curve represents the average separation between the holes introduced by doping. From Thurston, Birgeneau, Kastner *et al.* (1989).

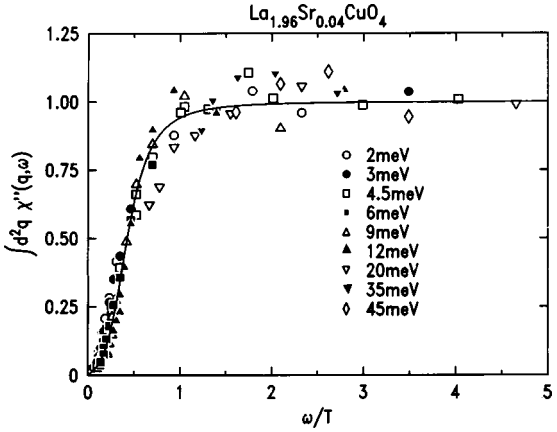

FIG. 35. Normalized integrated spin susceptibility as a function of the scaling variable ω/T. The solid curve is the function $(2/\pi)\tan^{-1}[a_1(\omega/T) + a_3(\omega/T)^3]$ with $a_1 = 0.43$ and $a_3 = 10.5$. From Keimer *et al.* (1991).

relation:

$$\kappa(x,T)=\kappa(x,0)+\kappa(0,T), \tag{7.2}$$

where $\kappa(0,T)$ is the temperature-dependent inverse of the correlation length of the undoped system given by Eq. (4.7) with $2\pi\rho_s = 150$ meV. The solid curves in Fig. 33 correspond to Eq. (7.2) with $\kappa(x,0)$ fixed by the low-temperature data, corresponding to $\xi = 150$, 65, and 42 Å, for the $x = 0.02$, 0.03, and 0.04 samples, respectively. For $\xi > 150$ Å, found in samples with hole concentrations less than 0.02, the residual anisotropic and interplanar interactions precipitate a transition to 3D long-range order. For $\xi < 150$ Å, only 2D short-range order is seen down to 10 K. This behavior is very different from that expected from the nonlinear sigma model in the quantum disordered regime (Chakravarty *et al.*, 1988; Chakravarty *et al.*, 1989; Keimer, Belk *et al.*, 1992; Sokol *et al.*, 1994).

The growth of $\kappa(x,0)$ with Sr content, seen in Fig. 33, is quite significant. This growth continues as one enters the superconducting regime of the phase diagram for $x > 0.05$ (Fig. 1). Figure 34 shows the data of Thurston, Birgeneau, Kastner, *et al.* (1989) for the low-temperature value of $\xi = \kappa^{-1}$ as a function of x. The solid curve is the average distance between the holes with no adjustable parameters. Quantitative analysis of the data in Fig. 34 shows that this relationship breaks down near $x \approx 0.02$, as it must since for smaller hole concentrations long-range order is achieved, that is, $\kappa \to 0$.

In addition to the resistance being linear in T, which occurs for x as small as ~ 0.02, another feature characteristic of superconducting crystals is seen in the spin glass regime. In a detailed study of the spin dynamics of $La_{1.96}Sr_{0.04}CuO_4$, Keimer *et al.* (1991) found remarkably simple scaling behavior of the q-integrated imaginary part of the susceptibility. The experiment involves measuring at fixed energy the intensity integrated around the (1,0,0) position [or equivalently (π,π) in square lattice unit lattice-constant notation] as a function of T. Keimer *et al.* found that the relation

$$\chi''(\omega)=\int_{\pi,\pi} d^2q\ \chi''(\mathbf{q},\omega)=I(|\omega|,0)\ \frac{2}{\pi}\arctan \times\left[a_1\left(\frac{\omega}{T}\right)+a_3\left(\frac{\omega}{T}\right)^3\right] \tag{7.3}$$

describes all of the data quite well. The quantity $\chi''(\omega)/I(|\omega|,0)$ is plotted as a function of ω/T in Fig. 35; the solid line is Eq. (7.3).

The scaling behavior described by Eq. (7.3) has been found in a number of materials, including $La_{1.95}Ba_{0.05}CuO_4$ (Hayden *et al.*, 1991), $La_{1.98}Sr_{0.02}CuO_4$ (Matsuda *et al.*, 1993), $YBa_2Cu_{2.9}Zn_{0.1}O_{6.6}$ (Kakurai *et al.*, 1993), $YBa_2Cu_3O_{6.5}$ with the superconducting $T_c = 53$ K (Birgeneau *et al.*, 1992), and $YBa_2Cu_3O_{6.6}$ with $T_c = 53$ K (Sternlieb *et al.*, 1993). Recently, Aeppli *et al.* (1997) demonstrated ω/T scaling in the normal state of optimally doped $La_{1.86}Sr_{0.14}CuO_4$ and related this to a putative nearby quantum critical point. In the superconductors, the T dependence is different from that predicted by Eq. (7.3) below T_c. Aside from this, the primary difference between the materials is in the ω dependence of $I(|\omega|,0)$. For the superconductors, $I(|\omega|,0)$ increases, approximately proportionally, with ω at small ω, whereas for the nonsuperconductors it decreases with increasing ω. We discuss this in more detail below.

It is important to emphasize that there is no difference in the scaling behavior of χ'' above and below 100 K in the crystal of $La_{1.96}Sr_{0.04}CuO_4$ (Fig. 35), whose resistivity (in Fig. 29) reaches a minimum near 100 K. Thus $\chi''(q,\omega)$, as well as the instantaneous correlation function, is insensitive to localization effects, as one might expect since the localization length for this sample is ~100 Å and the inelastic scattering length approaches this length only at very low T.

Keimer *et al.* (1991) point out that the simplest model consistent with relaxational dynamics in a disordered antiferromagnet gives

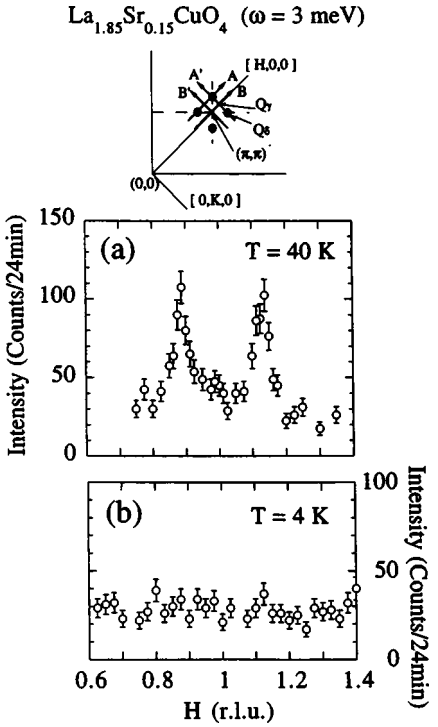

FIG. 36. Neutron inelastic scattering spectra at 3 meV at temperatures above and below the superconducting transition temperature of $T_c = 37.3$ K. The measurement was made at an energy transfer of 3 meV along the direction labeled A in the schematic drawing (top) of reciprocal space near (π,π). The closed circles denote the peak positions of the incommensurate magnetic fluctuations. From Yamada *et al.* (1995).

$$\chi(q,\omega)=\frac{\xi^2}{1+q^2\xi^2-iF(\omega/\Gamma)}. \tag{7.4}$$

In mean-field theory one finds $\Gamma \sim \xi^2$, which is incompatible with our observation (Fig. 33) that the correlation length is independent of temperature below ~ 300 K, whereas χ'' is certainly not. Thus models that ascribe the scaling to the T dependence of ξ are clearly suspect. On the other hand, a variety of models appear to lead to the scaling of Eq. (7.3). For example, Varma *et al.* (1989) recognized quite early that a number of unusual properties of the high-T_c materials could stem from behavior of χ'' such as that of Eq. (7.3). One possible origin of the ω/T scaling is a nearby quantum critical point, an example of which was discussed by Chakravarty, Halperin, and Nelson (1988, 1989).

C. Spin fluctuations in superconducting $La_{2-x}Sr_xCuO_4$

One of the most interesting features of the inelastic neutron scattering data is that for hole concentrations up to $p \sim 0.05$ per Cu, for which the materials are not superconducting, the spin fluctuation scattering remains commensurate at the (π,π) position. However, as p is increased above 0.05 there is a commensurate-incommensurate transition in the spin fluctuation geometry. This was originally discovered independently by Yoshizawa *et al.* (1988) and by Birgeneau *et al.* (1989). Later, Cheong *et al.* (1991) discovered that at low energy

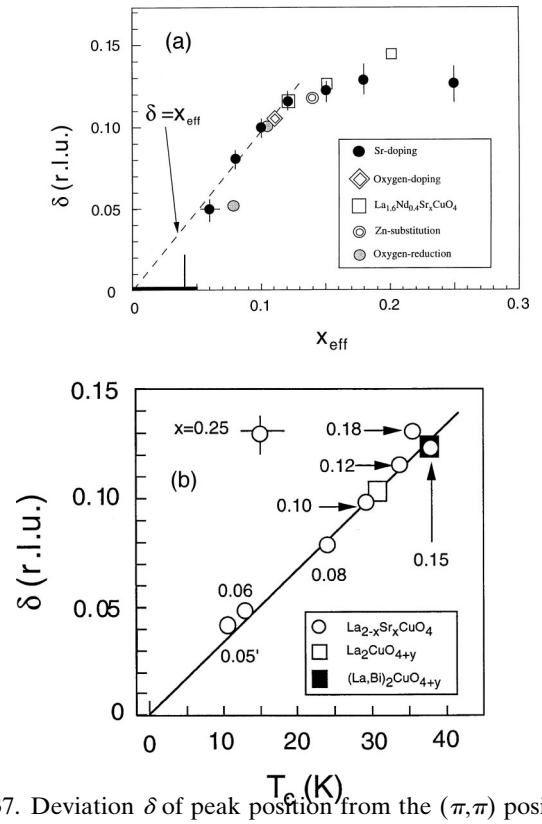

FIG. 37. Deviation δ of peak position from the (π,π) position (cf. Fig. 36) for crystals doped in a number of different ways: (a) plotted as a function of $x_{\rm eff}$ the fraction of excess holes per Cu atom resulting from both Sr and O doping, (b) plotted as a function of the superconducting transition temperature T_c.

and low T, the incommensurate scattering corresponds to four 2D rods at $(\pi \pm 2\pi\delta,\pi)$ and $(\pi,\pi \pm 2\pi\delta)$ symmetrically distributed about the antiferromagnetic (π,π) position, as illustrated in Fig. 36. In $YBa_2Cu_3O_{7-z}$ the width of the scattering makes it difficult to observe any incommensurability (Rossat-Mignod *et al.*, 1993; Sato *et al.*, 1993), although recently incommensurability in underdoped $YBa_2Cu_3O_{7-z}$, analogous to that in $La_{2-x}Sr_xCuO_4$ but rotated by 45° seems to have been observed (Dai *et al.*, 1998).

The hole concentration can be increased by doping with either oxygen or Sr; Yamada *et al.* (1998) call the fraction of holes per Cu atom resulting from both Sr and O doping $x_{\rm eff}$.

The dependence of δ on $x_{\rm eff}$ and $T_c(x_{\rm eff})$ is illustrated in Fig. 37. Remarkably, the incommensurability δ, while remaining zero up to $x_{\rm eff} = 0.05$, is proportional to T_c for $x_{\rm eff}$ up to the optimal value for all samples measured (Yamada *et al.*, 1998). Further, for $0.06 \leqslant x \leqslant 0.12$ one finds the simple quantitative relation $\delta = x$.

Since this incommensurate scattering is the main new feature that appears with doping into the superconducting phase, we discuss its behavior in more detail. To make the discussion simpler we treat the material as being effectively tetragonal. Then the rods at $(1,0,l)$ and $(1/2.1/2.l)$ intersect the $l = 0$ plane at the points (π,π) and $(0,\pi)$, respectively, in the 2D square lattice, unit lattice constant notation. The data we discuss were all taken with the sample oriented for scattering in the $(h,0,1)$ zone and tilted about the (0,0,1) axis by an angle

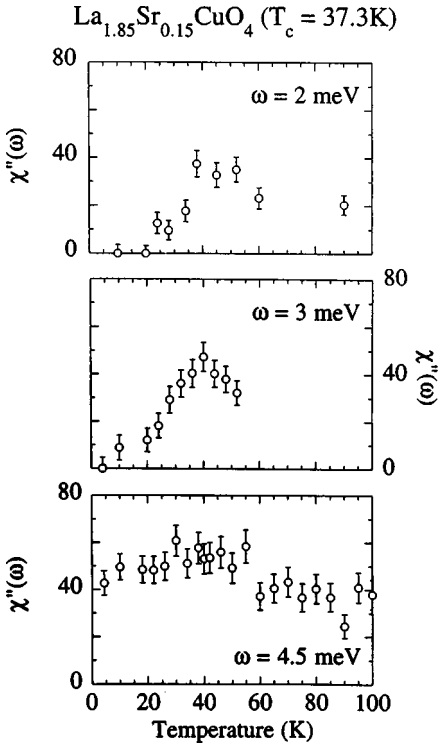

FIG. 38. Temperature evolution of $\chi''(q,\omega)$ at the incommensurate peak position for energies of 2 meV, 3 meV, and 4.5 meV. The data for 2 meV correspond to the 2D integral of the intensities around the peak. From Yamada *et al.* (1995).

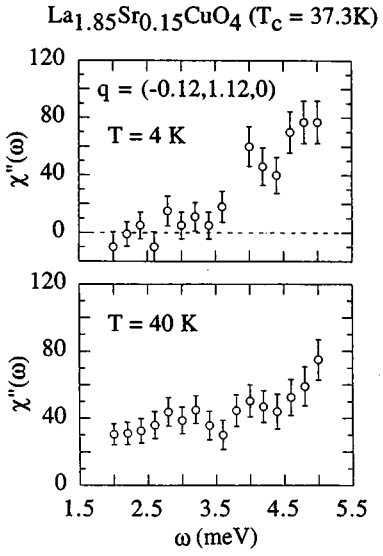

FIG. 39. The energy dependence of χ'' at the incommensurate peak for temperatures above and below $T_c = 37.3$ K. From Yamada *et al.* (1995).

of 6°. Because of the finite q resolution, this type of scan intersects two of the four rods, as illustrated by the trajectory in Fig. 36.

Matsuda *et al.* (1994) studied the temperature dependence of the incommensurate peaks for a crystal of $La_{1.85}Sr_{0.15}CuO_4$ with $T_c = 33$ K. Although the excitations are very sharp in q at low energies and change their temperature dependence as T is reduced below T_c, the incommensurate peaks persist in the superconducting phase. Quantitatively similar results have been obtained by Mason *et al.* (1993) on a sample of $La_{1.86}Sr_{0.14}CuO_4$. More recently, Wells *et al.* (1997) have studied the spin fluctuations in stage-6 $La_2CuO_{4.055}$ which has $T_c = 31$ K; this corresponds to a doping of ~ 0.11 holes per Cu atom. This stage-6 material exhibits spin fluctuations that are closely similar in all respects to those observed in the $La_{1.85}Sr_{0.15}CuO_4$, $T_c = 33$ K sample. This suggests that the underdoping is of fundamental importance in determining the spin dynamics. Recently, Yamada *et al.* (1995) have shown that for a crystal with $T_c = 37.3$ K, the behavior below T_c is quite different. Specifically, for $E < \sim 3.5$ meV the intensity of the incommensurate peaks as a function of T shows a sharp maximum at $T \sim T_c$ and diminishes rapidly toward zero as the temperature is lowered, indicating the opening of a gap for spin excitations.

Figure 36 shows a scan at $T = 40$ K, just above T_c, where two sharp incommensurate peaks are seen for $\omega = 3$ meV. However, at 4 K the peaks are not detectable above the background. Figure 38 shows the temperature dependence of χ''. The data at 2 meV correspond to an integral in q along a scan through the incommensurate peaks like the one in Fig. 36, while the results at 3 and 4.5 meV are simply the value of χ'' at one of the incommensurate peak positions. It is clear that for energies of both 2 and 3 meV, χ'' has a peak at $T \sim T_c = 37.3$ K and diminishes to zero as $T \to 0$. By contrast, at $\omega = 4.5$ meV, χ'' is approximately constant below T_c. This implies a magnetic gap energy between 3 and 4.5 meV. This should be contrasted with the superconducting BCS weak-coupling s-wave gap energy of $2\Delta = 3.54kT_c = 11.4$ meV. We note that the temperature dependence of χ'' at the incommensurate peak of $\omega = 2$ meV is similar to the behavior of $1/T_1T$ measured with NMR for ^{63}Cu (Oshugi *et al.*, 1991); this measures $\Sigma_q\chi''(\mathbf{q},\omega)/\omega$ in the limit $\omega \to 0$.

In Fig. 39 is shown the energy dependence of χ'' at the incommensurate peak position at $T = 4$ K and $T = 40$ K for two separate crystals. For $T = 40$ K, above T_c, χ'' varies gradually with energy, possibly going to zero as $\omega \to 0$. On the other hand, at $T = 4$ K, χ'' is nonzero above 3.5 meV but is not measurable above the background for lower energies. This shows that there is a superconducting magnetic gap of 3.5 ± 0.5 meV for the spin fluctuations at the incommensurate peak position in **q** space. Concomitantly, it also suggests that the low-energy spin scattering in the superconducting state for the crystals studied by Matsuda *et al.* (1994) and Mason *et al.* (1993) results from disorder and/or underdoping. Detailed analysis shows that the measured gap energy is consistent with $d_{x^2-y^2}$ models for the superconductivity provided $2\Delta_0 = 6kT_c$ (Zha *et al.*, 1993; Bulut and Scalapino, 1994; Tanamato *et al.*, 1994; Quinlan and Scalapino, 1995).

It is important to note that, although the incommensurate peaks are very sharp, the correlation length of the spin fluctuations is still short. When one measures the

instantaneous correlation length in an energy-integrating experiment, one still finds a length consistent with Fig. 34. The sharp peaks for low energies mean that these low-energy excitations have a dynamical coherence length that is larger than the correlation length.

Recently, Hayden and co-workers have extended the measurements of Matsuda *et al.* (1994) of $\chi''(\omega)$ from 20 meV up to $\sim$ 225 meV (Hayden *et al.*, 1996). They show in $La_{1.86}Sr_{0.14}CuO_4$ that $\chi''(\omega)$ is approximately constant between 10 and 30 meV and diminishes gradually with increasing energy up to $\sim$ 225 meV. The inelastic peaks in $\chi''(\mathbf{q},\omega)$ are somewhat broader in $\mathbf{q}$ at fixed ω in $La_{1.86}Sr_{0.14}CuO_4$ compared with those in La_2CuO_4. However, the $\mathbf{q}$-integrated response $\chi''(\omega)$ is typically comparable in magnitude in the superconductor and in the insulator. The most drastic changes occur below $\sim$ 10 meV, as originally noted by Mason *et al.* (1996) and Thurston, Birgeneau, Kastner, *et al.* (1989). Most recently, Mason *et al.* (1996) have noted in $La_{1.86}Sr_{0.14}CuO_4$ that for energies above $\sim$ 7.5 meV, $\chi''(\omega)$ increases with decreasing temperature below T_c and that at the 7.5 meV threshold the extra scattering that appears in the superconducting state appears to be quite sharp in $\mathbf{q}$.

Finally, Tranquada *et al.*, (1995, 1996, 1997) have studied the incommensurate spin fluctuations in samples of $La_{1.6-x}Nd_{0.4}Sr_xCuO_4$ with $x = 0.12$, 0.15, and 0.20. These samples are superconducting, with $T_c \approx 4$ K, 11 K, and 15 K, respectively. The Nd causes a change in the CuO_6 octahedron tilt directions from (110) as in the low-temperature orthorhombic (LTO) phase to (100) characteristic of the low-temperature tetragonal (LTT) phase, with the transition occurring at a temperature of roughly 70 K. Remarkably, they find that the dynamical incommensurate spin fluctuations observed previously in $La_{2-x}Sr_xCuO_4$ and La_2CuO_{4+y} condense out and become static with order over long distances. Importantly, in the sample with $x = 0.12$ they observe evidence for a charge-density wave at wavevector $(0,2\pi \pm 4\pi\delta)$, which is established at slightly higher temperatures than the spin density wave condensation temperature. They interpret these results in terms of the frustrated phase separation charge stripe model of Emery and Kivelson (Kivelson and Emery, 1993; Emery and Kivelson, 1994).

The condensation of the spin fluctuations in $La_{1.6-x}Nd_{0.4}Sr_xCuO_4$ observed by Tranquada *et al.* (1995, 1996, 1997) is unrelated to the superconductivity. Indeed such a condensation had been observed earlier in samples of $La_{2-x}Sr_xCuO_4$ (Sternlieb *et al.*, 1990; Keimer, Belk, *et al.*, 1992) that were not superconducting and where the magnetic response was commensurate. In this case the correlation lengths were quite short (20–40 Å), whereas in the Nd-Co-doped samples studied by Tranquada *et al.* (1995, 1996, 1997) the correlation lengths exceeded 150 Å. Recently, Hirota *et al.* (1998a; 1998b) have observed the condensation of incommensurate quasielastic peaks below $\sim$ 30 K in samples of $La_{1.86}Sr_{0.14}Cu_{0.988}Zn_{0.012}O_{4+y}$ that were either superconducting ($T_c = 19$ K, $y = 0$) or, after annealing in Ar, nonsuperconducting ($y = -0.004$). In both cases, the magnetic order extended over intermediate distances $\sim$70 Å. The overall behavior of the magnetic fluctuations, both static and dynamic, seemed to be independent of the superconductivity, and indeed mirrored the behavior seen by Sternlieb *et al.* (1990) and Keimer, Belk, *et al.* (1992) in samples in the spin-glass concentration region. Finally, very recently Kimura and coworkers (Kimura *et al.*, 1998; Suzuki *et al.*, 1998) and Lee *et al.* (1998) have observed transitions to incommensurate long-range order (correlation lengths >200 Å) in $La_{1.88}Sr_{0.12}CuO_4$ ($T_c = 31$ K) and stage-4 La_2CuO_{4+y} ($T_c = 41$ K). In both cases the magnetic phase transition coincides with the onset of superconductivity; indeed in stage-4 La_2CuO_{4+y} the magnetic order parameter seems to follow the BCS form quite well. Thus in this case the superconducting and spin-density wave states are intimately related. In all of the cases discussed above, the static ordering wave vectors coincide with those of the low energy dynamical spin fluctuations.

Clearly, therefore, very rich behavior that does not seem to fall into a simple pattern is observed. Further experiments and theory will be required to determine the relationships between the superconductivity and the spin density waves, be they short or long range.

VIII. COUPLING BETWEEN MAGNETIC FLUCTUATIONS AND CONDUCTIVITY

Moriya *et al.* (1990) have proposed that the inelastic scattering of electrons is dominated by scattering from spin excitations. They argue that the resistance should then scale as

$$R \sim T \int_{-\infty}^{\infty} d\left[\frac{\hbar\omega}{kT}\right] \frac{\hbar\omega}{kT} \frac{e^{\hbar\omega/kT}}{(e^{\hbar\omega/kT}-1)^2} \int d^2Q\ \chi''(Q,\omega). \tag{8.1}$$

Obviously, any form of $\int d^2Q\chi''(Q,\omega)$ that is homogeneous in $\hbar\omega/kT$ will lead to resistance linear in T. Keimer, Belk, *et al.* (1992) showed that the measured $\chi''(Q,\omega)$ predicts a temperature dependence of the resistance that is in reasonable agreement with experiment.

The exchange interaction is so large in the CuO_2 layers that an external magnetic field has very little influence on the spin fluctuations. However, in the regime at low T where the log T dependence in seen, Preyer *et al.* (1991) have observed what they interpret to be suppression of spin fluctuation resistance by an external magnetic field. Instead of the highly anisotropic negative orbital magnetoresistance expected (Lee and Ramakrishnan, 1985) when weak localization is the origin of the log T dependence, Preyer *et al.* found isotropic negative magnetoresistance. Interaction effects cannot explain this either, for isotropic magnetoresistance from the latter is positive rather than negative. This means that the log T behavior has a new origin. The magnetoresistance approximately scales with H/T, and

while the similarity to the $\hbar\omega/kT$ scaling is suggestive, a detailed theoretical treatment is required to make this connection substantial.

IX. FINAL OBSERVATIONS

After a decade of research, there is still no consensus as to the correct theory of the new kind of superconductivity found in the copper oxides. In this section, we list some of the outstanding physics problems that are of fundamental interest in their own right and which may be important in arriving at the correct model for the superconductivity.

As discussed in Sec. V, the optical excitations above about 1.5 eV, seen in the absorption and reflection spectra of the undoped CuO_2 layer, are well understood. In the range 1.5–2 eV they correspond to excitons, which can be thought of as excitations of the d^9 hole between crystal-or ligand-field-split levels of the Cu^{2+} ions. Above 2 eV, they are charge-transfer excitations that result in large polarons. The sharp peak near 0.35 eV is now also explained. It corresponds to the creation of a two-magnon quasi-bound state together with an optical phonon. However, the broad features in the range 0.4–1 eV are apparently of mixed magnetic and excitonic nature. It appears that the $d_{3z^2-r^2}$ exciton lies at lower energy than predicted by cluster calculations. Several models for superconductivity have suggested an important role for such a low-lying exciton. Clearly, a better understanding of the nature of these low-lying excitations would be very valuable.

It is, at first, surprising that the electronic transport properties in the lightly doped limit are so ordinary. One might have expected the very strong coupling of the charge carriers to the magnetism to result in a heavy mass. The photoemission results show that the bandwidth for holes is, indeed, reduced from the several eV expected from band theory to of order $2J \sim 0.3$ eV. This indicates that the coupling of the hole to the antiferromagnetic background plays an essential role in determining the band structure. However, because the dispersion relation is strongly peaked, the effective mass at the top of the valence band is, nonetheless, relatively small, of order the free-electron mass. Since the holes, already coupled to the magnetic fluctuations, are subsequently dressed by phonons, the mass observed in transport measurements is somewhat heavier.

Other evidence of coupling between magnetism and transport comes from the work of Preyer, Birgeneau, Chen, *et al.* (1989) showing that there is a strong coupling between the interlayer hopping and the magnetism. However, the large magnetic correlation length, even at temperatures well above the Néel temperature, makes it unlikely that any effect of the magnetic order on the in-plane transport can be seen.

The polaronic properties of the charge carriers are very important. If the carriers are still polarons in the superconductor, as suggested by Capizzi *et al.* and others (Mihailovic *et al.*, 1990; Mihailovic *et al.*, 1991; Calvani *et al.*, 1994; Capizzi *et al.*, 1994), many ideas about the origins of the superconductivity may need to be modified.

Many features of the magnetism must be taken into account in any complete theory of the high-T_c superconductors. The scaling of χ'' with ω/T is a quite universal property of the superconductors. That this and the resistivity linear in T emerge at doping levels of only a few percent, in the spin-glass region where there is no superconductivity, is very important. Indeed, the only feature that is unique to the doped La_2CuO_4 superconductors is the incommensurate nature of the spin fluctuations. Clearly, experiments on samples closer to the commensurate-incommensurate transition are needed.

ACKNOWLEDGMENTS

The work at MIT was supported by the MRSEC Program of the National Science Foundation under award number DMR 94-00334 and by NSF award numbers DMR 94-1174 and DMR 97-04532. The neutron work was supported by the U.S.-Japan Cooperative Neutron Scattering Program. Research at Brookhaven National Laboratory was supported by the Division of Material Science of the Office of Basic Energy Science of the U.S. Department of Energy under Contract No. DE-AC-2-76CH00016. The work at Tohoku University was supported by a Grant-In-Aid for Scientific Research from the Japanese Ministry of Education, Science and Culture.

REFERENCES

Aeppli, G., S. M. Hayden, H. A. Mook, Z. Fisk, S.-W. Cheong, D. Rytz, J. P. Remeika, G. P. Espinosa, and A. S. Cooper, 1989, Phys. Rev. Lett. **62**, 2052.

Aeppli, G., T. E. Mason, S. M. Hayden, H. A. Mook, and J. Kulda, 1997, Science **278**, 1432.

Aharony, A., R. J. Birgeneau, A. Coniglio, M. A. Kastner, and H. E. Stanley, 1988, Phys. Rev. Lett. **60**, 1330.

Ando, Y., G. S. Boebinger, A. Passner, T. Kimura, and K. Kishio, 1995, Phys. Rev. Lett. **75**, 4662.

Ando, Y., G. S. Boebinger, A. Passner, K. Tamasaku, N. Ichikawa, S. Uchida, M. Okuya, T. Kimura, J. Shimoyama, and K. Kishio, 1996, J. Low Temp. Phys. **105**, 867.

Appel, J., 1968, in *Solid State Physics: Advances in Research and Applications*, Vol. 21, edited by F. Seitz, D. Turnbull, and H. Ehrenreich (Academic, New York), pp. 193–391.

Axe, J. D., A. H. Moudden, D. Hohlwein, D. E. Cox, K. M. Mohanty, A. R. Moodenbaugh, and Y. Xu, 1989, Phys. Rev. Lett. **62**, 2751.

Ballhausen, C. J., 1962, *Introduction To Ligand Field Theory* (McGraw-Hill, New York).

Beard, B. B., R. J. Birgeneau, M. Greven, and U.-J. Wiese, 1998, Phys. Rev. Lett. **80**, 1742.

Bednorz, J. G., and K. A. Müller, 1986, Z. Phys. B **64**, 189.

Belinicher, V. I., A. L. Chernyshev, and V. A. Shubin, 1996, Phys. Rev. B **54**, 14 914.

Bianconi, A., A. C. Casatellano, M. DeSantis, P. Rudolf, P. Lagarde, A. M. Flank, and A. Marcelli, 1987, Solid State Commun. **63**, 1009.

Birgeneau, R. J., A. Aharony, N. R. Belk, F. C. Chou, Y. Endoh, M. Greven, S. Hosoya, M. A. Kastner, C. H. Lee, Y. S. Lee, G. Shirane, S. Wakimoto, B. O. Wells, and K. Yamada, 1995, J. Phys. Chem. Solids **56**, 1913.

Birgeneau, R. J., C. Y. Chen, D. R. Gabbe, H. P. Jenssen, M. A. Kastner, C. J. Peters, P. J. Picone, T. Thio, T. R. Thurston, H. L. Tuller, J. D. Axe, P. Böni, and G. Shirane, 1987, Phys. Rev. Lett. **59**, 1329.

Birgeneau, R. J., Y. Endoh, Y. Hidaka, K. Kakurai, M. A. Kastner, T. Murakami, G. Shirane, T. R. Thurston, and K. Yamada, 1989, Phys. Rev. B **39**, 2868.

Birgeneau, R. J., R. W. Erwin, P. M. Gehring, M. A. Kastner, B. Keimer, M. Sato, S. Shamoto, G. Shirane, and J. Tranquada, 1992, Z. Phys. B **87**, 15.

Blakemore, J. S., 1969, *Solid State Physics* (W. B. Saunders, Philadelphia).

Boebinger, G. S., Y. Ando, A. Passner, T. Kimura, M. Okuya, J. Shimoyama, K. Kishio, K. Tamasaku, N. Ichikawa, and S. Uchida, 1996, Phys. Rev. Lett. **77**, 5417.

Böni, P., J. D. Axe, G. Shirane, R. J. Birgeneau, C. Y. Chen, D. R. Gabbe, H. P. Jenssen, M. A. Kastner, C. J. Peters, P. J. Picone, T. Thio, and T. R. Thurston, 1988, Phys. Rev. B **38**, 185.

Bringley, J. F., S. S. Trail, and B. A. Scott, 1990, J. Solid State Chem. **86**, 310.

Brooks, H., 1955, in *Advances in Electronics and Electron Physics*, edited by L. Marton (Academic, New York), Vol. 7.

Budnick, J. I., B. Chamberland, D. P. Yang, C. Niedermayer, A. Golnik, E. Recknagel, M. Rossmanith, and A. Weidinger, 1988, Europhys. Lett. **5**, 651.

Bulut, N., and D. J. Scalapino, 1994, Phys. Rev. B **50**, 16 078.

Calvani, P., M. Capizzi, S. Lupi, P. Maselli, A. Paolone, P. Roy, S.-W. Cheong, W. Sandowski, and E. Walker, 1994, Solid State Commun. **91**, 113.

Capizzi, M., S. Lupi, P. Calvani, P. Maselli, A. Paolone, P. Roy, H. Berger, and G. Balestrino, 1994, Physica C **273**, 235.

Chaillout, C., J. Chenavas, S. W. Cheong, Z. Fisk, M. Marezio, B. Morosin, and J. E. Schirber, 1990, Physica C **170**, 87.

Chaillout, C., S. W. Cheong, Z. Fisk, M. S. Lehmann, M. Marezio, B. Morosin, and J. E. Schirber, 1989, Physica C **158**, 183.

Chakravarty, S., B. I. Halperin, and D. R. Nelson, 1988, Phys. Rev. Lett. **60**, 1057.

Chakravarty, S., B. I. Halperin, and D. R. Nelson, 1989, Phys. Rev. B **39**, 2344.

Chattopadhyay, D., and H. J. Queisser, 1981, Rev. Mod. Phys. **53**, 745.

Chen, C. Y., R. J. Birgeneau, M. A. Kastner, N. W. Preyer, and T. Thio, 1991, Phys. Rev. B **43**, 392.

Chen, C. Y., E. C. Branlund, C. Bae, K. Yang, M. A. Kastner, A. Cassanho, and R. J. Birgeneau, 1995, Phys. Rev. B **51**, 3671.

Chen, C. Y., N. W. Preyer, P. J. Picone, M. A. Kastner, H. P. Jenssen, D. R. Gabbe, A. Cassanho, and R. J. Birgeneau, 1989, Phys. Rev. Lett. **63**, 2307.

Cheong, S.-W., G. Aeppli, T. E. Mason, H. Mook, S. M. Hayden, P. C. Canfield, Z. Fisk, K. N. Clausen, and J. L. Martinez, 1991, Phys. Rev. Lett. **67**, 1791.

Chou, F. C., N. R. Belk, M. A. Kastner, R. J. Birgeneau, and A. Aharony, 1995, Phys. Rev. Lett. **75**, 2204.

Chubukov, A., and S. Sachdev, 1993, Phys. Rev. Lett. **71**, 169.

Collins, R. T., Z. Schlesinger, G. V. Chandiashekar, and M. W. Shafer, 1989, Phys. Rev. B **39**, 2251.

Crawford, M. K., R. L. Harlow, E. M. McCarron, W. E. Farneth, J. D. Axe, H. Chou, and Q. Huang, 1991, Phys. Rev. B **44**, 7749.

Dai, P., H. A. Mook, and F. Dogan, 1998, Phys. Rev. Lett. **80**, 1738.

Ding, H.-Q., and M. S. Makivic, 1990, Phys. Rev. Lett. **64**, 449.

Eder, R., Y. Ohta, and G. A. Sawatzky, 1997, Phys. Rev. B **55**, R3414.

Elstner, N., A. Sokol, R. R. P. Singh, M. Greven, and R. J. Birgeneau, 1995, Phys. Rev. Lett. **75**, 938.

Emery, V. J., and S. A. Kivelson, 1994, Physica C **235–240**, 189.

Endoh Y. *et al.*, 1988, Phys. Rev. B **37**, 7443.

Eskes, H., L. H. Tjeng, and G. A. Sawatzky, 1990, Phys. Rev. B **41**, 288.

Falck, J. P., A. Levy, M. A. Kastner, and R. J. Birgeneau, 1992, Phys. Rev. Lett. **69**, 1109.

Falck, J. P., A. Levy, M. A. Kastner, and R. J. Birgeneau, 1993, Phys. Rev. B **48**, 4043.

Falck, J. P., J. D. Perkins, A. Levy, M. A. Kastner, J. M. Graybeal, and R. J. Birgeneau, 1994, Phys. Rev. B **49**, 6246.

Feynman, R. P., 1955, Phys. Rev. **97**, 660.

Freltoft, T., G. Shirane, S. Mitsuda, J. P. Remeika, and A. S. Cooper, 1988, Phys. Rev. B **37**, 137.

Fritzsche, H., 1955, Phys. Rev. **99**, 406.

Fritzsche, H., 1978, in *The Metal Non-metal Transition in Disordered Systems: Proceedings of The Nineteenth Scottish Universities Summer School in Physics, St. Andrew, 1978*, edited by L. R. Friedman and D. P. Tunstall (Scottish Universities Summer School in Physics, Edinburgh), p. 193.

Fritzsche, H., and M. Cuevas, 1960, Phys. Rev. **119**, 1238.

Ganguly, P., and C. N. R. Rao, 1984, J. Solid State Chem. **53**, 193.

Glazman, L. I., and A. S. Ioselevich, 1989, Pis'ma Zh. Éksp. Teor. Fiz. **49**, 503.

Gold, A., 1991, Phys. Rev. B **44**, 8818.

Goodenough, J. B., and A. Manthiram, 1990, J. Solid State Chem. **88**, 115.

Gooding, R. J., 1991, Phys. Rev. Lett. **66**, 2266.

Gooding, R. J., and A. Mailhot, 1993, Phys. Rev. B **48**, 6132.

Gooding, R. J., N. M. Salem, R. J. Birgeneau, and F. C. Chou, 1997, Phys. Rev. B **55**, 6360.

Grande, V. B., H. Müller-Buschbaum, and M. Schwerzer, 1977, Z. Anorg. Allg. Chem. **428**, 120.

Greven, M., R. J. Birgeneau, Y. Endoh, M. A. Kastner, B. Keimer, M. Matsuda, G. Shirane, and T. R. Thurston, 1994, Phys. Rev. Lett. **72**, 1096.

Greven, M., R. J. Birgeneau, Y. Endoh, M. A. Kastner, M. Matsuda, and G. Shirane, 1995, Z. Phys. B **96**, 465.

Grilli, M., C. Castellani, and C. Di Castro, 1990, Phys. Rev. B **42**, 6233.

Grüninger, M., J. Münzel, A. Gaymann, A. Zibold, H. P. Geserich, and T. Kopp, 1996, Europhys. Lett. **35**, 55.

Harris, A. B., and S. Kirkpatrick, 1977, Phys. Rev. B **16**, 542.

Harshman, D. R., G. Aeppli, B. Batlogg, G. P. Espinosa, R. J. Cava, A. S. Cooper, and L. W. Rupp, 1989, Phys. Rev. Lett. **63**, 1187.

Harshman, D. W., G. Aeppli, G. P. Espinosa, A. S. Cooper, J. P. Remeika, E. J. Ansaldo, and T. M. Riseman, 1988, Phys. Rev. B **38**, 852.

Hasenfratz, P., and F. Niedermayer, 1991, Phys. Lett. B **268**, 231.

Hayden, S. M., G. Aeppli, R. Osborn, A. D. Taylor, T. G. Perring, S.-W. Cheong, and Z. Fisk, 1991, Phys. Rev. Lett. **67**, 3622.
Hayden, S. M., G. Aeppli, and H. A. Mook, 1996, Phys. Rev. Lett. **76**, 1344.
Hidaka, Y., T. Enomoto, M. Suzuki, M. Oda, and T. Murakami, 1987, J. Cryst. Growth **85**, 581.
Hirochi, K., S. Hayashi, H. Adachi, T. Mitsuyu, T. Hirao, K. Setsune, and K. Wasa, 1989, Physica C **160**, 273.
Hirota, K., K. Yamada, I. Tanaka, and H. Kojima, 1998a, Institution Preprint.
Hirota, K., K. Yamada, I. Tanaka, and H. Kojima, 1998b, Institution Preprint.
Hosoya, S., T. Fukuda, T. Kajitani, K. Hiraga, K. Oh-ishi, Y. Syono, K. Yamada, Y. Endoh, T. Takahashi, and H. Katayama-Yoshida, 1992, Jpn. J. Appl. Phys. **7**, 81.
Iio, K., and K. Nagata, 1976, J. Phys. Soc. Jpn. **41**, 1550.
Imai, T., C. P. Slichter, K. Yoshimara, M. Katoh, and K. Kosuge, 1993, Phys. Rev. Lett. **71**, 1254.
Jorgensen, J. D., B. Dabrowski, S. Pei, D. G. Hinks, L. Soderholm, B. Morosen, J. E. Schriber, F. L. Venturini, and D. S. Ginley, 1988, Phys. Rev. B **38**, 11 337.
Kakurai, K., S. Shamoto, T. Kiyokura, M. Sato, J. M. Tanquada, and G. Shirane, 1993, Phys. Rev. B **48**, 3485.
Keimer, B., A. Aharony, A. Auerbach, R. J. Birgeneau, A. Cassanho, Y. Endoh, R. W. Erwin, M. A. Kastner, and G. Shirane, 1992, Phys. Rev. B **45**, 7430.
Keimer, B., N. Belk, R. J. Birgeneau, A. Cassanho, C. Y. Chen, M. Greven, M. A. Kastner, A. Aharony, Y. Endoh, R. W. Erwin, and G. Shirane, 1992, Phys. Rev. B **46**, 14 034.
Keimer, B., R. J. Birgeneau, A. Cassanho, Y. Endoh, R. W. Erwin, M. A. Kastner, and G. Shirane, 1991, Phys. Rev. Lett. **67**, 1930.
Keimer, B., R. J. Birgeneau, A. Casanho, Y. Endoh, M. Greven, M. A. Kastner, and G. Shirane, 1993, Z. Phys. B **91**, 373.
Kim, C., P. J. White, Z.-X. Shen, T. Tohyama, Y. Shibata, S. Maekawa, B. O. Wells, Y. J. Kim, R. J. Birgeneau, and M. A. Kastner, 1998, Phys. Rev. Lett. **80**, 4245.
Kim, Y. H., S. W. Cheong, and Z. Fisk, 1991, Phys. Rev. Lett. **67**, 2227.
Kimura, H., K. Hirota, K. Yamada, S. H. Lee, C. F. Majkrzak, R. Erwin, and R. J. Birgeneau, 1998, Institution Preprint.
Kitaoka, Y., K. Ishida, T. Kobayashi, K. Amaya, and K. Asayama, 1988, Physica C **153–155**, 733.
Kivelson, S. A. and V. J. Emery, 1993, edited by K. S. Bedell *et al.* (Addison Wesley, Redwood City), p. 619.
Kopietz, P., 1990, Phys. Rev. Lett. **64**, 2587.
Kumagai, K., I. Watanabe, H. Aoki, Y. Nakamura, T. Kimura, Y. Nakamichi, and H. Nakajima, 1987, Physica B & C **148**, 480.
Kyung, B., and R. A. Ferrell, 1996, Phys. Rev. B **54**, 10 125.
Laughlin, R. B., 1997, Phys. Rev. Lett. **79**, 1726.
Lee, P., and T. V. Ramakrishnan, 1985, Rev. Mod. Phys. **57**, 287.
Lee, T. K., and C. T. Shih, 1997, Phys. Rev. B **55**, 5983.
Lee, Y. S., M. A. Kastner, R. J. Christianson, R. J. Birgeneau, K. Yamada, Y. Endoh, and G. Shirane, 1998, unpublished.
Leung, P. W., B. O. Wells, and R. J. Gooding, 1998, Phys. Rev. B **56**, 6320.
Liu, R., D. Salamon, M. V. Klein, S. L. Cooper, W. C. Lee, S. W. Cheong, and D. M. Ginsberg, 1993, Phys. Rev. Lett. **71**, 3709.
Lorenzana, J., and G. A. Sawatzky, 1995a, Phys. Rev. Lett. **74**, 1867.
Lorenzana, J., and G. A. Sawatzky, 1995b, Phys. Rev. B **52**, 9576.
Lyons, K. B., P. A. Fleury, J. P. Remeika, A. S. Cooper, and T. J. Negran, 1988, Phys. Rev. B **37**, 2353.
Lyons, K. B., P. A. Fleury, L. F. Schneemeyer, and J. V. Waszczak, 1988, Phys. Rev. Lett. **60**, 732.
Lyons, K. B., P. A. Sulewski, P. A. Fleury, H. L. Carter, A. S. Cooper, and G. P. Espinosa, 1989, Phys. Rev. B **39**, 9693.
Makivic, M. S., and H.-Q. Ding, 1991, Phys. Rev. B **43**, 3562.
Marshall, W., and R. Lowde, 1968, Rep. Prog. Phys. **31**, 705.
Mason, T. E., G. Aeppli, S. M. Hayden, A. P. Ramirez, and H. A. Mook, 1993, Phys. Rev. Lett. **71**, 919.
Mason, T. E., A. Schroder, H. A. Mook, and S. M. Hayden, 1996, Phys. Rev. Lett. **76**, 1604.
Matsuda, M., R. J. Birgeneau, Y. Endoh, Y. Hidaka, M. A. Kastner, K. Nakajima, G. Shirane, T. R. Thurston, and K. Yamada, 1993, J. Phys. Soc. Jpn. **62**, 1702.
Matsuda, M., Y. Endoh, K. Yamada, H. Kojima, I. Tanaka, R. J. Birgeneau, M. A. Kastner, and G. Shirane, 1992, Phys. Rev. B **45**, 12 548.
Matsuda, M., K. Yamada, Y. Endoh, T. R. Thurston, G. Shirane, R. J. Birgeneau, M. A. Kastner, I. Tanaka, and H. Kojima, 1994, Phys. Rev. B **49**, 6958.
McMahan, A. K., J. F. Annett, and R. M. Martin, 1990, Phys. Rev. B **42**, 6268.
McMahan, A. K., R. M. Martin, and S. Satpathy, 1988, Phys. Rev. B **38**, 6650.
Mezei, F., B. Farago, C. Pappas, G. Hutiray, L. Rosta, and L. Mihaly, 1988, Physica C **153–155**, 1669.
Mihailovic, D., C. M. Foster, K. Voss, and A. J. Heeger, 1990, Phys. Rev. B **42**, 7989.
Mihailovic, D., C. M. Foster, K. F. Voss, T. Mertelj, I. Poberaj, and N. Herron, 1991, Phys. Rev. B **44**, 237.
Morgenstern, I., 1990, Z. Phys. B **80**, 7.
Moriya, T., Y. Takahashi, and K. Ueda, 1990, J. Phys. Soc. Jpn. **59**, 2905.
Nakajima, K., K. Yamada, S. Hosoya, Y. Endoh, M. Greven, and R. J. Birgeneau, 1995, Z. Phys. B **96**, 479.
Nazarenko, A., K. J. E. Vos, S. Haas, E. Dagotto, and R. J. Gooding, 1995, Phys. Rev. B **51**, 8676.
Oshugi, S., Y. Kitaoka, K. Ishida, and K. Asayama, 1991, J. Phys. Soc. Jpn. **60**, 2351.
Paalanen, M. A., T. F. Rosenbaum, G. A. Thomas, and R. N. Bhatt, 1983, Phys. Rev. Lett. **51**, 1896.
Perkins, J. D., R. J. Birgeneau, J. M. Graybeal, M. A. Kastner, and D. S. Kleinberg, 1998, Phys. Rev. B (in press).
Perkins, J. D., J. M. Graybeal, M. A. Kastner, R. J. Birgeneau, J. P. Falck, and M. Greven, 1993, Phys. Rev. Lett. **71**, 1621.
Perkins, J. D., D. S. Kleinberg, M. A. Kastner, R. J. Birgeneau, Y. Endoh, K. Yamada, and S. Hosoya, 1995, Phys. Rev. B **52**, R9863.
Picone, P., H. P. Jenssen, and D. R. Gabbe, 1988, J. Cryst. Growth **91**, 463.
Preyer, N. W., R. J. Birgeneau, A. Cassanho, C. Y. Chen, D. R. Gabbe, H. P. Jenssen, M. A. Kastner, P. J. Picone, and T. Thio, 1989, Physica C **162–164**, 1003.
Preyer, N. W., R. J. Birgeneau, C. Y. Chen, D. R. Gabbe, H. P. Jenssen, M. A. Kastner, P. J. Picone, and T. Thio, 1989, Phys. Rev. B **39**, 11 563.
Preyer, N. W., M. A. Kastner, C. Y. Chen, R. J. Birgeneau, and Y. Hidaka, 1991, Phys. Rev. B **44**, 407.

Quinlan, S. M., and D. J. Scalapino, 1995, Phys. Rev. B **51**, 497.
Rabe, K. M., and R. N. Bhatt, 1991, J. Appl. Phys. **69**, 4508.
Rossat-Mignod, J., L. P. Regnault, P. Bourges, P. Bartlet, C. Vettier, and J. H. Y. Henry, 1993, in *Frontiers in Solid State Science: Selected Topics in Superconductivity*, edited by L. C. Gupta and M. S. Multani (World Scientific, Singapore), p. 265.
Salamon, D., R. Liu, M. V. Klein, M. A. Karlow, S. L. Cooper, S.-W. Cheong, W. C. Lee, and D. M. Ginsberg, 1995, Phys. Rev. B **51**, 6617.
Samara, G. A., W. F. Hammetter, and E. L. Venturini, 1990, Phys. Rev. B **41**, 8974.
Sato, M., S. Shamoto, T. Kiyokura, K. Kakurai, G. Shirane, B. J. Sternlieb, and J. M. Tranquada, 1993, J. Phys. Soc. Jpn. **62**, 263.
Sera, M., Y. Ando, S. Kondoh, K. Fukuda, and M. Sato, 1989, Solid State Commun. **69**, 851.
Serre, J., A. Ghazali, and A. Gold, 1989, Phys. Rev. B **39**, 8499.
Shirane, G., Y. Endoh, R. J. Birgeneau, M. A. Kastner, Y. Hidaka, M. Oda, M. Suzuki, and T. Murakami, 1987, Phys. Rev. Lett. **59**, 1613.
Shklovskii, B. I., and A. L. Efros, 1984, *Electronic Properties of Doped Semiconductors* (Springer, Berlin).
Shraiman, B. I., and E. D. Siggia, 1988, Phys. Rev. Lett. **61**, 467.
Shraiman, B. I., and E. D. Siggia, 1989a, Phys. Rev. B **40**, 9162.
Shraiman, B. I., and E. D. Siggia, 1989b, Phys. Rev. Lett. **62**, 1564.
Singh, R. R. P., P. A. Fleury, K. B. Lyons, and P. E. Sulewski, 1989, Phys. Rev. Lett. **62**, 2736.
Sokol, A., R. Glenister, and R. R. P. Singh, 1994, Phys. Rev. Lett. **72**, 1549.
Sternlieb, B. J., G. M. Luke, Y. J. Uemura, T. M. Riseman, J. H. Brewer, P. M. Gehring, K. Yamada, Y. Hidaka, T. Murakami, T. R. Thurston, and R. J. Birgeneau, 1990, Phys. Rev. B **41**, 8866.
Sternlieb, B. J., G. Shirane, J. M. Tranquada, M. Sato, and S. Shamoto, 1993, Phys. Rev. B **47**, 5320.
Sugai, S., T. Kobayashi, and J. Akimitzu, 1989, Phys. Rev. B **40**, 2686.
Sugai, S., and M. Sato, 1989, Phys. Rev. B **40**, 9292.
Sugai, S., M. Sato, T. Kobayashi, J. Akimitsu, T. Ito, H. Takagi, S. Uchida, S. Hosoya, T. Kajitani, and T. Fukuda, 1990, Phys. Rev. B **42**, 1045.
Suzuki, T., T. Goto, K. Chiba, T. Shinoda, T. Fukase, H. Kimura, K. Yamada, M. Ohashi, and Y. Yamaguchi, 1998, Phys. Rev. B **57**, R3229.
Takagi, H., B. Batlogg, H. L. Kao, J. Kwo, R. J. Cava, J. J. Krajewski, and J. W. F. Peck, 1992, Phys. Rev. Lett. **69**, 2975.
Tanaka, I., and H. Kojima, 1989, Nature (London) **337**, 21.
Tanamato, T., H. Kohno, and H. Fukuyama, 1994, J. Phys. Soc. Jpn. **63**, 2739.
Thio, T., and A. Aharony, 1994, Phys. Rev. Lett. **73**, 894.
Thio, T., R. J. Birgeneau, A. Cassanho, and M. A. Kastner, 1990, Phys. Rev. B **42**, 10 800.
Thio, T., C. Y. Chen, B. S. Freer, D. R. Gabbe, H. P. Jenssen, M. A. Kastner, P. J. Picone, N. W. Preyer, and R. J. Birgeneau, 1990, Phys. Rev. B **41**, 231.
Thio, T., T. R. Thurston, N. W. Preyer, P. J. Picone, M. A. Kastner, H. P. Jenssen, D. R. Gabbe, C. Y. Chen, R. J. Birgeneau, and A. Aharony, 1988, Phys. Rev. B **38**, 905.
Thomas, G. A., 1991, in *High Temperature Superconductivity*, edited by D. P. Tunstall and W. Barford (Adam Hilger, Bristol), p. 169.
Thomas, G. A., D. H. Rapkine, S. L. Cooper, S.-W. Cheong, A. S. Cooper, L. F. Schneemeyer, and J. V. Waszczak, 1992, Phys. Rev. B **45**, 2474.
Thurston, T. R., R. J. Birgeneau, D. R. Gabbe, H. P. Jenssen, M. A. Kastner, P. J. Picone, N. W. Preyer, J. D. Axe, P. Böni, G. Shirane, M. Sato, K. Fukuda, and S. Shamoto, 1989, Phys. Rev. B **39**, 4327.
Thurston, T. R., R. J. Birgeneau, M. A. Kastner, N. W. Preyer, G. Shirane, Y. Fujii, K. Yamada, Y. Endoh, Y. Hidaka, and T. Murakami, 1989, Phys. Rev. B **40**, 4585.
Tokura, Y., S. Koshihara, T. Arima, H. Takagi, S. Ishibashi, T. Ido, and S. Uchida, 1990, Phys. Rev. B **41**, 11 657.
Tranquada, J. M., J. D. Axe, N. Ichikawa, A. R. Moodenbaugh, Y. Nakamura, and S. Uchida, 1997, Phys. Rev. Lett. **78**, 338.
Tranquada, J. M., J. D. Axe, N. Ichikawa, Y. Nakamura, S. Uchida, and B. Nachumi, 1996, Phys. Rev. B **54**, 7489.
Tranquada, J. M., B. J. Sternlieb, J. D. Axe, Y. Nakamura, and S. Uchida, 1995, Nature (London) **375**, 561.
Uchida, S., T. Ido, H. Takagi, T. Arima, Y. Tokura, and S. Tajima, 1991, Phys. Rev. B **43**, 7942.
Uemura, Y. J. *et al.*, 1988, J. Phys. (Paris) **49**, 2087.
Vaknin, D., S. K. Sinha, D. E. Moncton, D. C. Johnston, J. M. Newsom, C. R. Safenya, and J. H. E. King, 1987, Phys. Rev. Lett. **58**, 2802.
Varma, C. M., P. B. Littlewood, S. Schmitt-Rink, E. Abraham, and A. E. Ruckenstein, 1989, Phys. Rev. Lett. **63**, 1996.
Villain, J., 1977, J. Phys. C **10**, 4793.
Villain, J., 1978, Z. Phys. B **33**, 31.
Wells, B. O., R. J. Birgeneau, F. C. Chou, Y. Endoh, D. C. Johnston, M. A. Kastner, Y. S. Lee, G. Shirane, J. M. Tranquada, and K. Yamada, 1996, Z. Phys. B **100**, 535.
Wells, B. O., Y. S. Lee, M. A. Kastner, R. J. Christianson, R. J. Birgeneau, K. Yamada, Y. Endoh, and G. Shirane, 1997, Science **277**, 1067.
Wells, B. O., Z.-X. Shen, A. Matsuura, D. M. King, M. A. Kastner, M. Greven, and R. J. Birgeneau, 1995, Phys. Rev. Lett. **74**, 964.
Xiang, T., and J. M. Wheatley, 1996, Phys. Rev. B **54**, R12 653.
Yamada, K., C. H. Lee, K. Kurahashi, J. Wada, S. Wakimoto, S. Ueki, H. Kimura, Y. Endoh, S. Hosoya, G. Shirane, R. J. Birgeneau, M. Greven, M. A. Kastner, and Y. J. Kim, 1998, Phys. Rev. B **57**, 6165.
Yamada, K., S. Wakimoto, G. Shirane, C. H. Lee, M. A. Kastner, S. Hosoya, M. Greven, Y. Endoh, and R. J. Birgeneau, 1995, Phys. Rev. Lett. **75**, 1626.
Yamada, N., M. Oda, M. Ido, Y. Okajima, and K. Yamaya, 1989, Solid State Commun. **70**, 1151.
Yoshizawa, H., S. Mitsuda, H. Kitazawa, and K. Katsumata, 1988, J. Phys. Soc. Jpn. **57**, 3686.
Zha, Y., K. Levin, and Q. Si, 1993, Phys. Rev. B **47**, 9124.
Zhang, F. C., and T. M. Rice, 1988, Phys. Rev. B **37**, 3759.